Akkermansia muciniphila identified as key strain to alleviate gut barrier injury through Wnt signaling pathway

Xin Ma [a,b], Meng Li [a,b], Yuanyuan Zhang [b], Tingting Xu [b], Xinchen Zhou [a,b], Mengqi Qian [b], Zhiren Yang [a,b], Xinyan Han [a,b,*]

[a] Hainan Institute of Zhejiang University, Yongyou Industry Park, Yazhou Bay Sci-Tech City, Sanya 572000, China

[b] Key Laboratory of Animal Nutrition and Feed Science in East China, Ministry of Agriculture, College of Animal Sciences, Zhejiang University, Hangzhou 310058, China

*Corresponding author

Xinyan Han

College of Animal Sciences, Zhejiang University, 866 Yuhangtang Road, Hangzhou 310058, China

E-mail: xyhan@zju.edu.cn

Credit author statement

XH and XM: Designed the experiments; XM and TX: Performed the experiments; XZ and MQ: Analyzed the data; XM and ML: Wrote the manuscript, which was edited by YZ, TX, MQ, XZ, ZY and HX. All authors read and approved the final manuscript.

ABSTRACT

As the largest mucosal surface, the gut has built a physical, chemical, microbial and immune barrier to protect the body against pathogen invasion**.** The disturbance of gut microbiota aggravates pathogenic bacteria invasion and gut barrier injury. Fecal microbiota transplantation (FMT) is a promising treatment for microbiome-related disorders, where beneficial strain engraftment is a significant factor influencing FMT outcomes. The aim of this research was to explore the effect of FMT on antibiotic-induced microbiome-disordered (AIMD) model infected with enterotoxigenic *Escherichia coli* (ETEC). We used piglet, mouse and intestinal organoid models to explore the protective effects and mechanisms of FMT on ETEC infection. The results showed that FMT regulated gut microbiota and enhanced the protection of AIMD piglets against ETEC K88 challenge, as demonstrated by reduced intestinal pathogen colonization and alleviated gut barrier injury. *Akkermansia muciniphila* (*A. muciniphila*) and *Bacteroides fragilis* (*B. fragilis*) were identified as two strains that may play key roles in FMT. We further investigated the alleviatory effects of these two strains on ETEC infection in AIMD mice model, which revealed that *A. muciniphila* and *B. fragilis* relieved ETEC-induced intestinal inflammation by maintaining the proportion of Treg/Th17 cells and epithelial damage by moderately activating the Wnt/β-catenin signaling pathway, while the effect of *A. muciniphila* was better than *B. fragilis*. We therefore identified whether *A. muciniphila* protected against ETEC infection using basal-out and apical-out intestinal organoid models. *A. muciniphila* did protect the intestinal stem cells and stimulate proliferation and differentiation of intestinal epithelium, and the protective effects of *A. muciniphila* was reversed by Wnt inhibitor. FMT alleviated ETEC-induced gut barrier injury and intestinal inflammation in AIMD model. *A. muciniph*ila was identified as key strain in FMT to promote proliferation and differentiation of intestinal stem cells by mediating the Wnt/β-catenin signaling pathway.

Keywords: *Akkermansia muciniphila*; Wnt/β-catenin signaling pathway; Apical-out intestinal organoids; Gut barrier injury; Fecal microbiota transplantation.

Introduction

Growing evidence suggests that gut microbiota and its metabolites play important roles in modulating host health (*Canfora et al., 2019; Ghosh et al., 2021; Zheng et al., 2021*). The most drastic exposure that leads to intestinal microbiota dysbiosis is antibiotic treatment, which kills commensal micro-organisms and inhibits these microbiota-mediated immune defense (*Andremont et al., 2021; Buffie and Pamer, 2013*). The disturbance of intestinal microbiota may lead to disruptions of gut barrier and increase the susceptibility of host to pathogenic microbes (*Flint et al., 2012; Witkowski et al., 2020*). Several clinical studies have demonstrated that early-life exposure to antibiotic leads to gut microbiota dysbiosis that can impair host immune system maturation (*An et al., 2014; Nguyen et al., 2020*). Furthermore, the negative impact of antibiotics on gut microbiota in early life may even last for long periods throughout a lifetime, increasing the risk of gut diseases (*Francino, 2016*). Enterotoxigenic *Escherichia coli* (ETEC) K88 infection is a common cause of diarrhea in humans and animals (*Dubreuil, 2021*). When ETEC adheres to intestinal epithelial cells, virulence factors interact with specific receptors to induce intestinal barrier injury and intestinal inflammatory responses (*Yu et al., 2018*). Fecal microbiota transplantation (FMT) is a therapeutic intervention for reconstructing gut microbiota in gastrointestinal inflammatory diseases (*Borody et al., 2019; Colman and Rubin, 2014*). Since FMT has been successful in treating *Clostridioides difficile* infection and maintaining gut barrier, emerging investigation has been focused on other diseases (*Quraishi et al., 2017*). However, whether FMT could remedy against ETEC K88 infection in antibiotic-induced gut microbiota-disordered (AIMD) piglets is still unknown. Simultaneously, the underlying mechanism of FMT and the gut microbes that confer its efficacy remain unclear.

Intestinal stem cell renewal is vital for the maintenance of gut barrier (*Beumer and Clevers, 2021*). Mammalian intestinal epithelial cells are renewed approximately every 3-5 days with the migration of undifferentiated intestinal cells from the crypt to the top of the villi, accompanied by the differentiation of different types of epithelial cells (*Luo et al., 2022*). The proliferation and differentiation of intestinal epithelium driven by intestinal stem cells, mainly

crypt base columnar cells expressing R-Spondin receptor Lgr5, is a necessary process for repairing intestinal barrier injury to prevent pathogen invasion (*Yan et al., 2017*). *Sato et al.* (*2009*) successfully cultured isolated intestinal stem cells into three-dimensional intestinal organoids with villous and crypt-like structural morphology for the first time. Intestinal organoids contain various terminally differentiated cell types, including intestinal stem cell, tuft cell, absorptive cell, enteroendocrine cell, goblet cell, and Paneth cell, which have more advantages over single cell lines for *in vitro* study of intestinal regeneration (*Sprangers et al., 2021*). Intestinal organoid is an ideal model for studying the interaction between intestinal epithelium and microorganisms in vitro, which can eliminate the complexity of animal models (*Yin et al., 2019*). In traditional basal-out intestinal organoid models, the intestinal epithelium was in the interior of organoid spheroid, which restricted the interaction between intestinal epithelium and gut microbiota. *Co et al.* (*2019*) first established the intestinal organoid model with polarity reversal in human and mouse, which optimizes the shortcomings of microinjection in terms of heterogeneous exposure concentrations and durations, as well as destruction of organoid walls, and evaluated the infection effects of the invasive pathogens with different polarity-specific patterns.

In the present study, we first investigated the effects of FMT on ETEC K88 infection in AIMD neonatal piglets, then by using bacterial 16S rDNA sequencing analysis, we identified *Akkermansia muciniphila* (*A. muciniphila*) as potential microbe to alleviate ETEC-induced intestinal barrier injury. We further hypothesized that *A. muciniphila* could relieve intestinal barrier injury and intestinal inflammation by modulating the proliferation and differentiation of intestinal epithelium, and verified this hypothesis using *in vivo* mice experiments as well as *in vitro* porcine intestinal organoid models. Collectively, our results may provide theoretical basis that *A. muciniphila* is a promising method to repair intestinal barrier damage and a new strategy for the precise application of *A. muciniphila* in livestock production.

Materials and methods

Ethics statement

All animal experiments were performed according to the guidelines of the Animal Care Committee of Zhejiang University School of Medicine (permit number SYXK 2012-0178). The animal care protocol was approved by the Local Committee of Animal Use following the Guide for the Care and Use of Laboratory Animals (NIH publication 86-23 revised 1985).

Preparation of fecal microbiota suspension and bacterial strains

The fecal microbiota suspension was prepared according to our previous method (*Ma et al., 2021*). In short, healthy adult Jinhua pigs that administrated medicinal feed additives or drugs for more than 3 months were selected as fecal donors. The potential risks and infectious pathogens in donor pigs were determined by serological and stool testing to ensure the safety of the porcine FMT. Fresh fecal samples that collected from Jinhua pigs were transported in AnaeroPack (Mitsubishi Gas Chemical, Japan) on ice to laboratory within 2 hours. The 50 g fecal samples were homogenized in 250 mL sterile phosphate-buffered saline solution (PBS), filtered through sterile stainless-steel strainer, and then centrifuged at 4000 rpm for 10 min. The precipitate was resuspended in sterile PBS solution containing 10% sterile glycerol, and the fecal microbiota suspension was stored at -80°C. All the above preparation was performed in an anaerobic incubator (AW400SG anaerobic workstations; Electrotek, UK). All the facilities and tools for the preparation of the fecal microbiota suspension were sterilized prior to use. When processing the FMT, the fecal microbiota suspension was thawed in 37°C water bath. ETEC K88 serotype O149:K91:K88ac was purchased from the China Institute of Veterinary Drug Control (Beijing China), cultured in Luria-Bertani medium (Qingdao Hope Bio-Technology Company, China), and incubated at 37□ in a shaker with 250 rpm overnight. *A. muciniphila* ATCC BAA-835 and *Bacteroides fragilis* (*B. fragilis*) ATCC 25285 were purchased from Guangdong Microbial Culture Collection Center (GDMCC, Guangzhou, China). *A. muciniphila* was cultured in brain heart infusion media (OXOID, Thermo Fisher Biochemicals Ltd., UK) supplemented with 0.1% mucin (Sigma-Aldrich, USA). *B. fragilis* was cultured in trypticase soy broth (Qingdao Hope Bio-Technology Company, China) supplemented with 5% defibrinated sheep blood (Qingdao Hope Bio-Technology Company,

China). These two anaerobic bacteria strains were incubated at 37□ in an anaerobic incubator with 10% H_2, 10% CO_2, and 80% N_2 (AW400SG anaerobic workstations; Electrotek, UK). The cultures were centrifuged for 10 min at a speed of 4000 rpm, and the pellets were then resuspended in either aerobic or anaerobic PBS.

Animals

A total of 9 litters (9-11 piglets per litter) of Duroc × Landrace × Yorkshire ternary hybrid neonatal piglets (aged 5 days) with identical birth dates and parities were obtained from Anji Lvjiayuan Animal Husbandry Co. Ltd. (Zhejiang, China). Piglets were individually housed in pens with appropriate environment of 24-26□ and 55-65% humidity. All newborn piglets were fed with artificial milk substitutes, in which the nutrients reached the requirements recommended by the National Research Council (NRC, 2012), and had *ad libitum* access to water.

A total of 130 female C57BL/6 mice aged 5 weeks were obtained from Shanghai SLAC Laboratory Animal, Co., Ltd. (SCXK (Zhejiang) 2017-0005; Shanghai, China). Mice were housed in vinyl isolators in a room with 23 ± 1□ room temperature, 55-65% humidity and 12 h/12 h light/dark schedule. All mice had free access to water and food.

Experimental design

The piglets were randomly assigned to three groups (three litters per group): the control group (Con group), the ETEC K88 + PBS group (EP group) and the ETEC K88 + FMT group (EF group). The piglets in EP and EF groups were orally inoculated with 2 ml ampicillin (120 mg kg^{-1}) twice daily on day 1-3 of the experiment to disorder the intestinal resident microbiota, then orally inoculated with ETEC K88 (1×10^9 CFU ml^{-1}) suspended in 2 ml sterile PBS once daily on day 4-6 of the experiment. After ETEC K88 infection, the piglets in EF group received 1.5 ml fecal microbiota suspension once daily by oral gavage for 6 days, while the piglets in EP group received the same volume of sterile PBS. Meanwhile, the piglets in Con group were orally inoculated with the same volume of sterile PBS throughout the

experiment. The doses of ampicillin and fecal microbiota suspension were based on a previous study by Ma et al. [18]. Experimental design of piglets is shown in Figure 1A. The weight of each piglet was measured at both the beginning and the end of the experiment to calculate the average daily gain (ADG), and diarrhea score (0, normal feces; 1, moist feces; 2, mild diarrhea; 3, severe diarrhea) was recorded throughout the experiment. Six piglets (2 piglets per litter) were picked from each group to be slaughtered at the end of the experiment (Day 13).

After acclimating for a week, mice were randomly assigned to four groups (n = 10 each): the control group (C group), the ETEC K88 + PBS group (E group), the ETEC K88 + *A. muciniphila* group (A group) and the ETEC K88 + *B. fragilis* group (B group). On day 1-3 of the experiment, the mice in E, A and B groups were orally inoculated with 0.2 ml 15 mg ml^{-1} ampicillin (Sigma-Aldrich, USA) twice daily to disorder the gut microbiota. On day 4-6 of the experiment, the mice in E, A and B groups were infected with ETEC K88 (1×10^9 CFU) suspended in 0.2 ml 0.1 M $NaHCO_3$ buffer (pH 9.0) by oral gavage once daily. Mice were fasted for 12 h before infection. Meanwhile, the mice in C group were given the equal volume of sterile PBS on day 1-6 of the experiment. On day 7-13 of the experiment, live *A. muciniphila* (1×10^6 CFU) and live *B. fragilis* (1×10^8 CFU) suspended in 0.2 ml anaerobic sterile PBS were administered intragastrically once daily to the mice in A group and B group respectively, while mice in C and E groups received the same volume of anaerobic sterile PBS. The design of mouse experiment is shown in Figure 1B. Mice were orally infused with 0.2 ml 40 mg ml^{-1} 4 kDa fluorescein isothiocyanate-dextran (Sigma-Aldrich, USA) 4 hours before sampling. At the end of the experiment (Day 14), six mice in each group were randomly selected for ether anesthesia and neck dislocation.

Culture and treatment of porcine intestinal organoid

The cryovial of porcine intestinal organoid was kindly provided by Professor Li Xiaoliang (Institute of Preventive Veterinary Medicine, College of Animal Sciences, Zhejiang University, Hangzhou, China). The frozen organoids were thawed in a 37□-water bath for 2

min, and then added 1 ml of DMEM/F-12 (Gibco, USA) with 1% bovine serum albumin (BSA, BioFroxx, Germany) solution. The contents of the cryovial were mixed and transferred to the 15 ml conical tube containing 2 ml of DMEM/F-12 with 1% BSA solution, and then centrifuged at 200 × g for 5 min at 4□. The organoids were resuspended in equal volume of complete IntestiCult™ Organoid Growth Medium (06010, StemCell™ Technologies, Canada) and Matrigel Matrix (356231, Corning, USA). The 50 μl of the 500-crypt suspension was plated in the center of each well of the pre-warmed 24-well plate (3524, Corning, USA). The plate was placed at 37□ with 5% CO_2 for 10 min and then added 750 μl complete IntestiCult™ Organoid Growth Medium containing 100 μg ml^{-1} penicillin/streptomycin (Invitrogen, USA) to each well. The culture medium was fully exchanged three times per week. For the treatment, the frozen organoids were passaged two times after thawing.

For generation of apical-out organoids, the procedure of reversing the polarity of organoids was performed according to a previously published protocol by *Co et al.* (*2021*). Briefly, after growing in Matrigel Matrix with growth medium for 7 days, the Matrigel-embedded organoids were gently dissolved with 500 μl cold 5 mM ethylene diamine tetraacetic acid (EDTA) in D-PBS and transferred to the 15 ml conical tube containing 10 ml of cold 5 mM EDTA. The tubes were incubated on a rotating platform at 4□ for 1 h, and then centrifuged at 200 × g for 3 min at 4□. The organoids were resuspended in complete IntestiCult™ Organoid Growth Medium containing 100 μg ml^{-1} penicillin/streptomycin and transferred to ultra-low attachment 24-well plate (3473, Corning, USA). The suspended organoids were cultured at 37□ with 5% CO_2 for 3 days.

To induce intestinal damage, the culture medium of basal-out and apical-out organoids was changed to DMEM/F-12 containing ETEC K88 (10^6 CFU). After the invasion for 1 h, the organoids were transferred to DMEM/F-12 containing 200 μg ml^{-1} penicillin/streptomycin for 1 h to kill residual extracellular bacteria. Then, the organoids were incubated in DMEM/F-12 containing *A. muciniphila* (10^5 CFU) for 1 h to detect the repair effect of *A. muciniphila*. In addition, the organoids in WNT-C59 group were pretreated with the Wnt inhibitor Wnt-C59 (100 nM, AdooQ, China) for 24 h prior to damage. After co-cultivation, the organoids were

collected and resuspended in 4% paraformaldehyde (PFA, Servicebio, China) at 4□ or RNAiso Plus (Takara, Japan) at -80□ for further analysis. For epithelial barrier integrity, the apical-out organoids were resuspended in a solution of 4 kDa fluorescein isothiocyanate-dextran (FD4) (2 mg ml^{-1}) diluted in DMEM/F-12 without phenol red. The design of organoids' experiment is shown in Figure 1C.

Real-time quantitative PCR (RT-qPCR) analysis

Total RNA from intestinal tissue and organoids was extracted using TRIzol method according to the precise instructions and cDNA was synthesized using PrimeScript™ RT Master Mix (Takara, Japan). With cDNA as template, RT-qPCR was performed using TB Green® *Premix Ex Taq*™ (Takara, Japan) on a LightCycler 480 System (Roche, Germany). The real-time primers used in this study are listed in Table S1. The relative mRNA expression of target genes was statistically analyzed based on the $2^{-\Delta\Delta Ct}$ method.

Bacterial load and intestinal permeability analyses

The bacterial load of ETEC K88 in piglets' jejunal and colonic mucosa was determined by the absolute quantification. In brief, the gene of ETEC K88 (Genbank Accession: M25302.1) was amplified by PCR (mK88-F: GGAATGGAAAGTTGGTACAGGTCTT, mK88-R: CCGGCATAAGATGCATTCACTTTC), and the PCR product was analyzed by agarose gel electrophoresis. The specific band was excised and recovered, connected with pGM-T vector, and transformed into high-efficiency chemoreceptor DH-5α cells. After culturing, the plasmid DNA was extracted and sequenced. The RT-qPCR analysis was performed as the description of section 2.5. The copy number of samples was calculated by the copy number of standard and the standard curve.

For the detection of ETEC K88 load in mice, fresh feces, jejunum and colon tissue, liver, spleen and kidney were homogenized in sterile normal saline using a tissue homogenizer (Jingxin Industrial Development Co., Ltd., China), then the homogenates were diluted 10-fold continuously, and the dilutions were plated on MacConkey Agar (Qingdao Hope Bio-

Technology Company, China). After incubating in aerobic incubator at 37□ for 24 h, the plates were counted three times. The results were presented as Lg CFU g^{-1} of samples.

For intestinal permeability assessment in mice, the serum fluorescence was detected using a SpectraMax M5 plate reader (Molecular Devices, USA) at a 485 nm excitation wavelength and a 535 nm emission wavelength. The standard curve was established from the fluorescence of FD4 at concentrations of 0.005, 0.01, 0.02, 0.04, 0.08, 0.16 0.32, 0.64, 1.28, 2.56, 5.12 and 10.24 μg ml^{-1} to calculate the FD4 concentration.

For detection of epithelial barrier integrity in organoids, the apical-out organoids in the FD4 solution were transferred to the slide and instantly imaged live by the laser scanning confocal microscope IX81-FV1000 (Olympus, Japan) with FV10-ASW software (Olympus, Japan).

Histology and morphology analyses

Jejunum and colon tissues were collected, fixed in 4% PFA, dehydrated with gradient alcohol and embedded in paraffin. The tissue sections were stained with hematoxylin-eosin (H&E) solution. The indexes related to the morphology of jejunum and colon were measured by using Image Plus (v6.0). Scanning electron microscopy (SEM) and transmission electron microscopy (TEM) were performed according to the procedure of the Bio-ultrastructure Analysis Lab of the Analysis Center of Agrobiology and Environmental Sciences, Zhejiang University. In brief, intestinal tissues were fixed in 2.5% glutaraldehyde, washed with PBS three times, postfixed with 1% OsO4 for 1 h, then dehydrated with gradient alcohol (30%, 50%, 70%, 80%, 90%, 95% and 100%) for about 15 min at each step. For SEM, the samples were dehydrated in Hitachi Model HCP-2 critical point dryer, coated with gold-palladium in Hitachi Model E-1010 ion sputter, and observed in Hitachi Model SU-8010 SEM. For TEM, the infiltrated samples were embedded in Spurr resin, sectioned in LEICA EM UC7 ultratome, and sections were stained by uranyl acetate and alkaline lead citrate, then observed in Hitachi Model H-7650 TEM.

Immunofluorescence analysis

Jejunum tissues were fixed in 4% PFA, dehydrated, paraffin embedded and sectioned. After antigen retrieval and blocking, the sections were incubated in primary antibodies at 4□ overnight and secondary antibodies at room temperature for 50 min in the dark, followed by staining with DAPI at room temperature for 10 min in the dark. The fixed organoids were incubated in primary antibodies in blocking/permeabilization buffer at room temperature for 4 h, and then incubated in secondary antibodies together with DAPI and phalloidin (Servicebio, China) in blocking/permeabilization buffer at room temperature for 2 h in the dark. The fluorescence images were captured using a laser scanning confocal microscope IX81-FV1000 (Olympus, Japan) combined with FV10-ASW software (Olympus, Japan). The information of primary and secondary antibodies is shown in Table S2.

Western blot analysis

Total protein was extracted by radioimmunoprecipitation assay lysis buffer and protein concentration was determined by a BCA Assay Kit (Thermo Fisher Scientific, USA). Equal protein amounts (60 μg) were electrophoresed on 10% sodium dodecyl sulphate-polyacrylamide gel and the separated proteins were transferred onto the polyvinylidene difluoride membranes (Millipore, USA) The membranes were blocked with Tris-buffered saline with Tween (TBST) containing 5% BSA for 1 h at room temperature, and incubated with the primary antibodies (Table S3) in TBST containing 3% BSA overnight at 4□. After several times washes in TBST, the membranes were incubated with secondary antibodies (Table S3) in TBST containing 3% BSA for 1 h at room temperature. The protein bands were visualized using SuperSignal® West Dura Extended Duration Substrate (Thermo Fisher Scientific, USA), and quantified by Image J software.

Microbiome sequencing analysis

Total DNA was extracted from intestinal contents using the E.Z.N.A. ®Stool DNA Kit (D4015, Omega, Inc., USA) according to the manufacturer's instructions. The quality of DNA

was detected by agarose gel electrophoresis, and total DNA was quantified by ultraviolet spectrophotometer. Specific primers 341 F (5'-CCTACGGGNGGCWGCAG-3') and 805 R (5'-GACTACHVGGGTATCTAATCC-3') were used for bacterial PCR amplification of 16S rDNA V3-V4 hypervariable region. The PCR products were purified using AMPure XT beads (Beckman Coulter Genomics, USA) and quantified by Qubit (Invitrogen, USA). The amplicon pools were prepared for sequencing and the size and quantity of the amplicon library were assessed on Agilent 2100 Bioanalyzer (Agilent, USA) and the Library Quantification Kit for Illumina (Kapa Biosciences, USA), respectively. The libraries were sequenced on NovaSeq PE250 platform. Samples were sequenced on an Illumina NovaSeq platform according to the manufacturer's recommendations. Paired-end reads were assigned to samples based on their unique barcode and truncated by cutting off the barcode and primer sequence. Paired-end reads were merged using FLASH. Quality filtering on the raw reads were performed under specific filtering conditions to obtain the high-quality clean tags according to the fqtrim (v0.94). Chimeric sequences were filtered using Vsearch software (v2.3.4). After dereplication using DADA2, the Operational Taxonomic Unit (OTU) were constructed by Amplicon Sequence Variants to obtain the final feature table and feature sequence. Species annotation of OTU sequences was performed using the Mothur method with the SSUrRNA database of Silva 132, and multiple sequence alignment was performed using MUSCLE (v3.8.31) software to obtain the phylogenetic relationships of all OTUs sequences. The data of each sample were normalized using a standard of sequence number corresponding to the sample with the least sequences. Subsequent analysis of alpha diversity and beta diversity were all performed based on the output normalized data. Alpha diversity is applied in analyzing complexity of species diversity for a sample through 4 indices, including Chao1, Observed species, Shannon, Simpson, and all these indices in our samples were calculated with QIIME2. Beta diversity was calculated by QIIME2, and the Anosim, principal coordinate analysis (PCoA) and non-metric multidimensional scaling (NMDS) analyses were drawn implemented through R software (v3.5.2) with anosim, WGCNA, stats, ggplot2 and

vegan packages. Linear discriminant analysis (LDA) effect size (LEfSe) package was used for LEfSe analysis. Other diagrams were implemented by using the R software (v3.5.2).

Quantification of Short chain fatty acids

The colonic contents (50 mg) were homogenized with 0.5 ml dH_2O in ball mill and then centrifuged. The supernatant 1 (0.3 ml) was homogenized with 0.5 ml dH_2O and then centrifuged. The supernatant 2 (0.5 ml) combined with supernatant 1 were mixed with 0.8 ml of 2-Methylvaleric acid as internal standard solution and 0.1 ml 50% H_2SO_4. After centrifuging, the supernatant was transferred into fresh glass vial for Gas chromatography-mass spectrometry analysis, which was performed using an Agilent 7890B gas chromatograph system coupled with an Agilent 5977B mass spectrometer. Short chain fatty acids (SCFA) were identified and quantified by the retention time and standard curves of the standard solutions.

Flow cytometry (FC) analysis

Intestinal lamina propria cells were isolated by using Mouse Lamina Propria Dissociation Kit (Miltenyi Biotec, Germany) according to the instruction. For cell surface staining, the cells were incubated with FC block at 2-8□ for 15 min, then were stained with Live/Dead Dye (FVS510, BD Pharmingen, USA) at room temperature for 15 min, followed by washing with Stain Buffer. Cells were incubated with specifical fluorescent antibodies (Table S4) at 2-8□ for 30 min to label immune cells. For intracellular factor staining, cells were fixed and permeabilized using Transcription Factor Fix/Prem Buffer at 4□ for 40 min, washed with 1 × Perm/Wash Buffer, and stained with intracellular markers at 4□ for 30 min. The stained cells were washed and resuspended in PBS, and assessed by the 12-color FACSCelesta flow cytometer (Becton, Dickinson and Company, USA). The single cells were first gated on SSC-A vs FSC-A and FSC-A vs FSC-H, and then $CD45^+Live^+$ cells were gated on single cells. The $CD45^+CD3^-$ cells were gated on $CD45^+Live^+$ cells. The $CD4^+$ T cells ($CD3^+CD4^+$ cells) were gated on $CD45^+CD3^-$ cells, Tregs ($CD25^+Foxp3^+$ cells), and Th17

355 cells ($CD4^+ROR\gamma t^+$ cells) were gated on $CD3^+CD4^+$ cells. The $CD86^+CD11C^+$ cells were
356 gated on DC^+CD3^- cells. The data were analyzed using FlowJo software (v10.8.0).
357
358 **Isolation and culture of mouse intestinal crypts**
359 The jejunum proximal to the stomach was harvested immediately after mice were
360 sacrificed. After gently flushing with cold D-PBS (without calcium and magnesium) using
361 injection syringe, the intestinal segment was opened longitudinally and gently washed with
362 cold D-PBS three times. Then, the washed intestine was cut into 2 mm pieces with scissors,
363 which fell into a 50 ml conical tube containing 15 ml cold D-PBS. The rinsing procedure that
364 using the 10 ml serological pipette to gently pipette the intestinal pieces up and down three
365 times and then aspirate off the supernatant and add 15 ml fresh cold D-PBS was repeated 10-
366 15 times until the supernatant was clear. The intestinal pieces were resuspended in 25 ml
367 Gentle Cell Dissociation Reagent (GCDR, StemCell™ Technologies, Canada) and incubated
368 at room temperature for 15 min on a rocking platform. After incubation, the intestinal pieces
369 were resuspended in 10 ml cold D-PBS containing 0.1% BSA, supernatant was filtered
370 through a 70 μm filter (Corning, USA), and filtrate was collected and labeled as fraction 1.
371 Repeat the above step three times to obtain fractions 2-4. The fractions were centrifuged at
372 290 × g for 5 min at 4□ and resuspended in 10 ml cold DMEM/F-12 with 15 mM HEPES.
373 The quality of the fractions was assessed by using an inverted microscope. The fraction which
374 enriched for intestinal crypts was selected, centrifuged and resuspended in equal volume of
375 complete IntestiCult™ Organoid Growth Medium (06005, StemCell™ Technologies, Canada)
376 and Matrigel Matrix. The 50 μl of the 500-crypt suspension was plated in the center of each
377 well of the pre-warmed 24-well plate. The plate was placed at 37□ with 5% CO_2 for 10 min
378 and then added 750 μl complete IntestiCult™ Organoid Growth Medium containing 100 μg
379 ml^{-1} penicillin/streptomycin to each well. The culture medium was fully exchanged three
380 times per week. After 7 to 10 days of culture, the organoids were passaged using 1:6 split ratio.
381 The images of organoids were captured using inverted microscope (Nikon, Japan). The
382 surface areas of organoids were measured using ImageJ software (v1.8.0). The forming

383 efficiency (%) = (number of mature organoids growing after 5 days / number of crypts seeded)
384 × 100%.
385
386 **Statistical analysis**
387 Data were statistically analyzed by SPSS (v26.0) software, and all data are presented as
388 means ± standard deviation (SD). *P* value < 0.05 was considered significant. Kolmogorov-
389 Smirnov test was used to determine whether the data followed the normal distribution.
390 Comparisons between two groups were executed by unpaired Student's *t*-test or Mann-
391 Whitney *U*-test, and comparisons among three groups were executed by one-way ANOVA or
392 Kruskal-Wallis followed by Dunn's multiple comparisons.
393
394 **Results**
395 **FMT enhanced the protection of AIMD piglets against ETEC K88 challenge**
396 ETEC K88 infection is a leading cause of diarrhea in humans and animals. We set out to
397 explore whether FMT protected against ETEC K88 challenge. The piglets were randomly
398 assigned to three groups: the control piglets (Con group), the ETEC K88 infected piglets (EP
399 group) and the ETEC K88 infected piglets with FMT treatment (EF group). As shown in
400 Figure 2A and 2B, decreased ADG and increased diarrhea score were observed in AIMD
401 piglets at day 3 and day 6 after ETEC K88 infection, and these symptoms were relieved by
402 FMT treatment. We next detected the pathogen colonization in mucosal tissues and found that
403 FMT significantly decreased the copies of ETEC K88 in the jejunal and colonic mucosa
404 (Figure 2C). To address whether FMT could protect intestinal barrier against ETEC K88
405 infection, intestinal barrier integrity and inflammatory cytokine levels were detected. FMT
406 decreased the expression of proinflammatory cytokines (*TNF-α*, *IL-1β* and *IL-6*) and
407 increased levels of anti-inflammatory cytokines (*IL-10* and *TGF-β1*) in the jejunum ($P < 0.01$,
408 Figure 2D). Jejunal scanning electron microscopy showed that the villi (Figure 3A top) in
409 ETEC K88 infected piglets were short and coarse, and there existed obvious rod-shaped
410 bacterial adhesion on the surface of microvilli (Figure 3A bottom), while FMT reversed villi

and microvilli injury caused by ETEC K88. In addition, the reduced mRNA and protein levels of the tight junctions (ZO-1, claudin and occludin) and adheren junctions (β-catenin and E-cadherin) caused by ETEC K88 challenge were also reversed by FMT treatment in the jejunum (Figure 3B-C). We then evaluated the expression of Mucin 2 (MUC2) in the jejunum using immunofluorescence staining. As shown in Figure 3D, ETEC K88 infection reduced the expression of MUC2, which was significantly increased following FMT administration. These results indicated that FMT enhanced the protection of AIMD piglets against ETEC K88 challenge.

A. muciniphila and _B. fragilis_ were identified as two key strains in FMT

We next assessed the variation of gut microbiota and SCFA metabolites in ETEC K88-challenged piglets. The alpha diversity indexes were increased after FMT treatment (Figure S1A-B). The PCoA and NMDS showed that gut microbiota between two groups clustered separately (Figure S1C-D). The Anosim analysis ($R = 0.396$, $P = 0.02$) and UPGMA clustering analysis also indicated that FMT altered the structure of the gut microbiota in ETEC K88-challenged piglets (Figure 4A-B). LEfSe analysis verified that *B. fragilis* and *Akkermansia* were changed significantly with an upper 4 LDA score after FMT administration (Figure 4C). We compared the OTU sequence of *Akkermansia* in the National Center for Biotechnology Information database by using Blast method based on Best Hit algorithm, and the result was *A. muciniphila*. Furthermore, FMT significantly increased the production of SCFA metabolites, including acetic acid, propionic acid, butyric acid, isobutyric acid, isovaleric acid and hexanoic acid (Figure 4D). These results demonstrated that FMT regulated gut microbiota and SCFA metabolites in ETEC K88-challenged piglets. *A. muciniphila* and *B. fragilis* were identified as two strains that may play key roles in FMT.

A. muciniphila and _B. fragilis_ maintain intestinal barrier function of ETEC-induced mice

We further investigated whether these two strains exerted protective effects on ETEC infection in AIMD mice model. Mice were randomly assigned to four groups: the control mice (C group), the ETEC K88 infected mice (E group), the ETEC K88 infected mice treated with *A. muciniphila* (A group) and the ETEC K88 infected mice treated with *B. fragilis* (B group). As shown in Figure S2A and 5A, ETEC K88 infection led to weight loss and intestinal morphology damage, which was relieved by *A. muciniphila* and *B. fragilis* treatment. Correspondingly, scanning electron microscopy showed that *A. muciniphila* and *B. fragilis* increased the height and number of microvilli and ameliorated the distribution of intercellular junction in the jejunum and colon (Figure 5B). In addition, the relative mRNA and protein expressions of MUC2 were significantly increased in the jejunum of *A. muciniphila* and *B. fragilis* treated mice (Figure 5C). However, only *A. muciniphila* could upregulated MUC2 protein expression in the colon of treated mice (Figure 5C). Furthermore, we investigated the diffusion of ETEC K88 in feces and organs after infection. ETEC K88 infection surged the number of *Escherichia coli* in the feces, jejunum, colon, liver, spleen and kidney (Figure S2B). *A. muciniphila* and *B. fragilis* treatment dramatically decreased the amount of ETEC K88 in these tissues (Figure S2B), indicating a reduced translocation of ETEC K88 in the tissues and organs. The concentration of FD4 in the serum has been commonly used as an indicator of intestinal permeability. As shown in Figure S2C, *A. muciniphila* and *B. fragilis* significantly decreased serum FD4 concentration, indicating *A. muciniphila* and *B. fragilis* enhanced intestinal barrier integrity.

ETEC K88 adheres to intestinal epithelial cells and induces gut inflammation. As demonstrated in Figure 6A, ETEC K88 decreased the relative mRNA expression of anti-inflammatory cytokines *IL-10* and *TGF-β* and increased levels of pro-inflammatory cytokines *TNF-α*, *IL-1β*, *IL-6* and *IFN-γ*, which was reversed in A and B groups, indicating that *A. muciniphila* and *B. fragilis* ameliorated ETEC K88-induced intestinal inflammation. Intestinal inflammatory response is closely related to immune cells. Treg cells secrete anti-inflammatory cytokines IL-10 and TGF-β to alleviate intestinal inflammation. Conversely, Th17 cells produce pro-inflammatory cytokines, such as IFN-γ and IL-17, which aggravate intestinal

466 inflammation. The dynamic balance of Treg and Th17 cells plays an important role in
467 intestinal immunity. Therefore, we used flow cytometry to analyze the proportion of the
468 immune cells isolated from jejunal lamina propria in the innate and adaptive immune system.
469 Treg cells were labeled with $CD25^+Foxp3^+$ cells, Th17 cells were labeled with $CD4^+ROR\gamma t^+$
470 cells, and mature dendritic cells were labeled with $CD86^+CD11C^+$ cells. ETEC K88 infection
471 significantly decreased the proportion of Treg cells and mature dendritic cells and increased
472 the proportion of Th17 cells, while oral administration of *A. muciniphila* or *B. fragilis*
473 significantly reduced the proportion of Th17 cells and increased the proportion of mature
474 dendritic cells (Figure 6B). Moreover, compared with E group, the proportion of Treg cells in
475 A group was significantly increased ($P < 0.01$), and the proportion of Treg cells in the B
476 group had an increasing trend ($P = 0.59$), indicating FMT maintained the proportion of
477 Treg/Th17 cells in ETEC K88-infected mice.
478
479 **_A. muciniphila_ accelerated intestinal epithelial proliferation**
480 Since oral administration of *A. muciniphila* and *B. fragilis* mitigated intestinal mucosal
481 injury, we set out to explore their effects on the proliferation and differentiation of intestinal
482 epithelium. ETEC K88 infection prominently decreased *Ki67* and *Lyz* mRNA expression and
483 the number of $Ki67^+$ cells and Lyz^+ Paneth cells in the crypt of the jejunum (Figure 7A and
484 7B). *A. muciniphila* and *B. fragilis* increased *Ki67* and *Lyz* mRNA expression and the number
485 of $Ki67^+$ cells. However, only *A. muciniphila* enhanced the number of Lyz^+ Paneth cells,
486 suggesting that *A. muciniphila* accelerated the proliferation and differentiation of intestinal
487 epithelial cells. Lgr5-labeled active intestinal stem cells are the driving force of intestinal
488 epithelial proliferation and differentiation after intestinal injury. ETEC K88 infection
489 significantly increased the relative mRNA expression of *Lgr5*, *Wnt3*, *Axin2*, *Ctnnb1* in
490 jejunum mucosa and had no significant impact on *Notch1* and *Hes1* expression (Figure 7C). *A.*
491 *muciniphila* and *B. fragilis* inhibited the upregulation of *Lgr5*, *Wnt3*, *Axin2* and *Ctnnb1* at
492 transcriptional level caused by ETEC K88 infection and had no significant effect on *Notch1*
493 and *Hes1* levels. Western blot analysis also showed that *A. muciniphila* and *B. fragilis*

494 inhibited the upregulation Lgr5, Wnt3, Active β-catenin, c-Myc and CyclinD1 at protein level,
495 and the effect of *A. muciniphila* was better than that of *B. fragilis* (Figure 7D). These results
496 implied that *A. muciniphila* regulated the expression of intestinal stem cells in ETEC K88-
497 challenged mice and regulated Wnt/β-catenin signaling pathway rather than Notch signaling
498 pathway.

499 We next isolated jejunal crypt from mice and explore whether *A. muciniphila* or *B.*
500 *fragilis* influenced the ability of intestinal stem cells growing into intestinal organoids *ex vivo.*
501 In ETEC K88-infected mice, the crypts formed into undifferentiated spherical organoids,
502 while in *A. muciniphila* or *B. fragilis* treated mice, the crypts generated mature organoids with
503 bud structure (Figure 8A). We statistically analyzed the surface area and forming efficiency of
504 the intestinal organoids. As shown in Figure 8B, the organoids derived from ETEC K88-
505 infected mice had smaller surface area and lower forming efficiency than those from control
506 mice. *A. muciniphila* treatment led to larger surface area and higher forming efficiency of the
507 intestinal organoids. The surface area of intestinal organoids in B group was larger than that in
508 E group, while there was no significant difference in forming efficiency between these two
509 groups. Meanwhile, the relative mRNA expression of genes related to the proliferation and
510 differentiation at the intestinal organoid level was consistent with the results of jejunal
511 mucosa *in vivo* (Figure 8C). These results suggested that *A. muciniphila* accelerated intestinal
512 epithelial proliferation and regulated Wnt/β-catenin signaling pathway *ex vivo*.
513
514 **_A. muciniphila_ protected intestinal organoids against ETEC infection via Wnt signaling**
515 To explore the effects and mechanisms of *A. muciniphila* on ETEC K88 infection *in vitro*,
516 the porcine intestinal organoids were infected with ETEC K88 (ETEC group), and then co-
517 cultured with *A. muciniphila* (AKK group). Wnt inhibitor Wnt-C59 was added to explore
518 whether *A. muciniphila* acted through Wnt/β-catenin signaling pathway (WNT-C59 group),
519 and porcine intestinal organoids without any treatment were used as blank control (CON
520 group). The relative mRNA expression of *villin*, *ZO-1*, *Ki67*, *Lyz*, *MUC2*, *Lgr5*, *Wnt3a*, *β-*
521 *catenin* and the fluorescence intensity of villin, Ki67, Lgr5, Wnt3a and β-catenin in basal-out

intestinal organoids were significantly down-regulated upon ETEC exposure (Figure 9A-G). *A. muciniphila* upregulated Lgr5, Wnt3a and β-catenin expression in ETEC-infected organoids, while these effects were inhibited by Wnt-C59 treatment (Figure 9A-G). The results suggested that *A. muciniphila* increased the number of intestinal stem cells and activated Wnt signaling, but did not promote the proliferation and differentiation of basal-out gut organoids. In basal-out intestinal organoid models, the intestinal epithelium was in the interior of organoid spheroid, which restricted the interaction between intestinal epithelium and *A. muciniphila*. Therefore, we reversed the polarity of basal-out intestinal organoids by removing the Matrigel from the culture system and suspending intestinal organoids in the culture (Figure S3A). In apical-out intestinal organoids, the apical surface was outward to make it accessible to *A. muciniphila*. Under confocal microscopy, the F-actin of basal-out intestinal organoid was located in the inside of the spheroids, while the F-actin of the apical-out intestinal organoid was outside the spheroids, indicating that the polar reversal intestinal organoid model was successfully constructed (Figure S3B). We conducted FD4 permeation test in apical-out intestinal organoid model, and co-cultivation with *A. muciniphila* restored the epithelial barrier integrity of organoids challenged by ETEC K88 (Figure 10A, H). *A. muciniphila* not only increased the mRNA expression of *ZO-1*, *Lyz* and *MUC2* in the ETEC K88 infected apical-out intestinal organoids, but also up-regulated the protein expression of villin, Wnt3a, β-catenin and the number of $Lgr5^+$ and $Ki67^+$ cells (Figure 10B-G, I). Moreover, *A. muciniphila* also relieved the inflammatory response of the ETEC K88 infected apical-out intestinal organoids, as determined by decreasing proinflammatory cytokines, inducing *TNF-α*, *IL-1β*, *IL-6* and *IFN-γ*, and increasing anti-inflammatory cytokines *IL-10* and *TGF-β* (Figure 10J). However, the moderating effect of *A. muciniphila* on the apical-out intestinal organoids disappeared after Wnt-C59 exposure. Taken together, *A. muciniphila* accelerated the proliferation and differentiation of the intestinal stem cells and ameliorated the intestinal barrier injury and inflammation induced by ETEC K88. *A. muciniphila* protected intestinal organoids against ETEC infection via Wnt signaling.

Discussion

The homeostasis of gut microbiota is a major contributor to host health. Intestinal dysbiosis increases intestinal colonization of antibiotic-resistant and pathogenic bacteria. Antibiotic treatment is the most drastic exposure leading to gut dysbiosis and pathogen invasion (*Andremont et al., 2021*). Early-life exposure to antibiotic leads to gut microbiota dysbiosis and impair host immune system maturation, which may even last for long periods throughout life (*Nguyen et al., 2020*). Researchers have made a lot of attempts to prevent or inhibit antibiotic-induced dysbiosis. Our previous study showed that FMT alleviates early-life antibiotic-induced gut microbiota dysbiosis and mucosa injuries in a neonatal piglet model (*Ma et al., 2021*). Our present study aimed to investigate whether FMT increases early-life antibiotic induced neonatal piglet against pathogen invasion. ETEC K88 is one of the most common pathogens in humans and animals and causes intestinal inflammation and diarrhea symptoms (*Sun and Kim et al., 2017*). Studies demonstrated that ETEC K88 infection led to pro-inflammatory cytokine upregulation and intestinal mucosal barrier injury (*Wang et al., 2020; Xie et al., 2021*). In ETEC-induced neonatal piglets, ZO-1 and Claudin-2 levels in ileum of were significantly decreased after ETEC K88 infection (*Xie et al., 2021*). In accordance with the above results, the present study showed that ETEC K88 infection increased the expression of pro-inflammatory cytokines and reduced the expression of intercellular junction proteins in AIMD piglets. Since FMT has been successful in treating *Clostridioides difficile* infection and maintaining gut barrier, emerging investigation has been focused on other diseases (*Cammarota et al., 2017*). *Geng et al.* (*2018*) demonstrated that FMT diminished the inflammatory response and the destruction of epithelial integrity in piglets challenged with lipopolysaccharide. In the present study, we found that FMT dampened ETEC K88-induced pro-inflammatory cytokines upregulation and improved the intestinal morphology. In addition, the number of ETEC K88 in jejunal and colonic mucosa was significantly decreased following FMT, which was consistent with the observation of jejunal microvilli under SEM, showing the absence of rod-shaped bacterial adhesion in FMT treatment. ETEC infection was reported to reduce the MUC2 expression by destroying goblet

578 cells or directly degrading MUC2, thereby damaging the integrity of the intestinal epithelial
579 barrier (*Luo et al., 2014*). Our results demonstrated that FMT enhanced the expression of
580 MUC2 and increased the expression of ZO-1, claudin, occludin, β-catenin and E-cadherin at
581 mRNA and protein levels, indicating that FMT improved the intercellular junctions between
582 intestinal epithelial cells and restored the integrity of the intestinal mucosal barrier to reduce
583 the colonization and invasion of ETEC K88.

584 Intestinal microbiota plays a key role in maintaining gut mucosal barrier and resistance
585 to pathogen invasion (*Chelakkot et al., 2018*). Antibiotic-induced gut microbiota-disorders
586 have been reported to disrupt gut barrier and increase the susceptibility of host to pathogenic
587 microbes (*Wlodarska et al., 2011*). So, we further probed the changes of gut microbiota in
588 AIMD piglets infected with ETEC K88. The results showed that FMT regulated gut
589 microbiota and SCFAs metabolism in ETEC K88-challenged piglets. LEfSe analysis
590 manifested that *B. fragilis* and *A. muciniphila* were the key differential bacteria between three
591 groups. *A. muciniphila* utilizes mucin as the only carbon and nitrogen source for its growth in
592 the gut, and its metabolite SCFAs can facilitate MUC2 secretion by goblet cells to maintain
593 the dynamic balance of intestinal mucus layer (*Ottman et al., 2017*). *A. muciniphila*
594 negatively correlated with many diseases, including diabetes, obesity and inflammatory bowel
595 diseases (*Belzer C and de Vos, 2012; Castro-Mejía et al., 2016; Plovier et al., 2017*). It has
596 been reported that *A. muciniphila* effectively inhibited intestinal inflammatory response and
597 elevated epithelial barrier function (*Everard et al., 2013; Li et al., 2016; Zhang et al., 2018*).
598 Meanwhile, *Bacteroides fragilis* is one of the symbiotic anaerobes within the mammalian gut
599 and is also an opportunistic pathogen which often isolated from clinical specimens (*Sun et al.,*
600 *2019*). Although it was initially thought to be pathogenic, in the long-term evolution process,
601 *Bacteroides fragilis* colonized in the gut has established a friendly relationship with the host,
602 which is an essential component for maintaining the health of the host, especially for obesity,
603 diabetes and immune deficiency diseases (*Troy and Kasper, 2010*). *B. fragilis* could
604 decompose mucin by lipid-anchored enzymes and interact with intestinal epithelial cells,
605 thereby altering intestinal permeability and repairing intestinal epithelial barrier (*Donaldson*

606 *et al., 2016; Hsiao et al., 2013*). *Deng et al.* (*2016*) reported that *B. fragilis* altered
607 macrophage phenotype and increased the phagocytosis of macrophages to restrain pathogens
608 colonization. Hence, we speculated that FMT increased the relative abundance of *A.*
609 *muciniphila* and *B. fragilis* in the intestine and alleviate intestinal barrier injury and intestinal
610 inflammation caused by ETEC K88 infection.

611 Since *A. muciniphila* and *B. fragilis* were identified as two strains that may play key
612 roles in FMT, we further investigate whether *A. muciniphila* and *B. fragilis* exerted protective
613 effect on ETEC K88 infection in AIMD mice model. We found that *A. muciniphila* and *B.*
614 *fragilis* maintained normal gut morphology after ETEC K88 infection, repaired the integrity
615 of intestinal mucosal barrier as evidenced by the reduced FD4 concentration in serum,
616 colonized in the intestine and inhibit the translocation of ETEC K88, and reduced the
617 intestinal inflammation, which may have been attributed to the increased proportion of Treg
618 cells and mature dendritic cells and the decreased proportion of Th17 cells. These results are
619 consistent with the protective role of *A. muciniphila* and *B. fragilis* in dextran sulphate sodium
620 salt induced enteritis model (*Bian et al., 2019; Wang et al., 2021; Zhai et al., 2019*). Intestinal
621 stem cell renewal is vital to maintaining the gut barrier. Ki67 is widely expressed in
622 proliferating cells and presents a reliable indicator of cell proliferation activity (*Zheng et al.,*
623 *2010*). Ki67 reaches its peak during the division stage with short half-life period and easy
624 degradation (*Zheng et al., 2010*). In our study, *A. muciniphila* and *B. fragilis* increased the
625 number of $Ki67^{+}$ cells and the mRNA expression of *Lyz*, suggesting that *A. muciniphila* and *B.*
626 *fragilis* accelerated the proliferation and differentiation of intestinal epithelium. Paneth cells
627 not only produce antimicrobial peptides and express key niche signals that regulate stem cells,
628 but also secrete activators that dynamically modulate Wnt/β-catenin signaling pathway (*Hou*
629 *et al., 2020*). The Wnt/β-catenin signaling pathway is essential for the proliferation and
630 differentiation of intestinal stem cells (*Ring et al., 2014*). When the Wnt receptors are
631 activated, the multiprotein degradation complex is rapidly inhibited, which allows β-catenin
632 to accumulate and subsequently migrate to the nucleus and binds to the transcription factors
633 of T cell factor family and lymphoid enhancer-binding factor family to drive the expression of

genes that regulate the stem cells, including Lgr5, c-Myc and Cyclin D1 (*Niehrs, 2012*). The c-Myc and Cyclin D1 are cyclins that positively regulate cell cycle from the G1 phase to S phase, thus inducing cell cycle progression and promote cell proliferation (*Shi et al., 2015*). *Zhu et al.* (*2020*) reported that *A. muciniphila* restored intestinal mucosal damage with the accelerated proliferation of intestinal epithelium through Wnt/β-catenin signaling pathway, thus relieving infection caused by *Salmonella pullorum* in chicks. In the present study, *A. muciniphila* moderately activated Wnt/β-catenin signaling pathway and maintain the suitable expression of Wnt, Active-β-catenin, Lgr5, c-Myc and Cyclin D1. Consistent with the *in vivo* results, *ex vivo* results of mouse intestinal organoids also demonstrated that *A. muciniphila* repaired the damaged intestinal epithelium caused by the ETEC K88 infection by modulating the Wnt/β-catenin signaling pathway. Simultaneously, *B. fragilis* also avoid the overactivation of the Wnt/β-catenin signaling pathway caused by the ETEC K88 infection, while the impact of *B. fragilis* was not as obvious as *A. muciniphila*.

Intestinal organoid is an ideal model for studying the interaction between intestinal epithelium and microorganisms in vitro, which can eliminate the complexity of animal models and avoid the unicity of the traditional intestinal epithelial cells (*Yin et al., 2019*). In order to further verify whether *A. muciniphila* attenuated ETEC K88 infection through Wnt/β-catenin signaling pathway, basal-out and apical-out porcine intestinal organoid models was used. Notably, we found that the ETEC K88 infection down-regulated Wnt/β-catenin signaling pathway *in vitro*, which was inconsistent with the results *in vivo*. A recent study showed that the addition of 400 ng ml^{-1} STp, an enterotoxin of ETEC, could suppress Wnt/β-catenin signaling pathway of porcine intestinal organoids (*Zhou et al., 2021*). It is speculated that the reason for the difference results might be related to the difference in the processing time of the *in vivo* and *in vitro* treatment. In spite of the slight stimulation of *A. muciniphila* on the proliferation and differentiation of infected intestinal organoids, *A. muciniphila* up-regulated the Wnt/β-catenin signaling pathway and had protective effects on intestinal stem cells. In basal-out intestinal organoid models, the intestinal epithelium was in the interior of organoid spheroid, which restricted the interaction between intestinal epithelium and *A. muciniphila*.

Co et al. (*2019*) first established the intestinal organoid model with polarity reversal in human and mouse and evaluated the infection effects of the invasive pathogens with different polarity-specific patterns, *Salmonella enterica serovar Typhimurium* and *Listeria monocytogenes*, on polarity reversal intestinal organoids. Subsequently, *Li et al.* (*2020*) first applied the porcine intestinal organoids with polarity reversal to investigate the infectivity and antiviral immune responses of porcine transmissible gastroenteritis virus. In addition, studies on host-pathogen interactions using polarity reversal intestinal organoids have also been reported in the sheep and chickens (). But up to now, there are few reports on the interaction between host and symbiotic microorganism using polarity reversal intestinal organoids. Here, we utilized porcine polarity reversal intestinal organoids to make *A. muciniphila* directly interacting with the intestinal epithelium. Our results showed that *A. muciniphila* alleviated the injury of polarity reversal intestinal organoids induced by ETEC K88. In agreement with the *in vivo* results, *A. muciniphila* restrain the intestinal inflammation caused by the ETEC K88 infection in polarity reversal intestinal organoids. Additionally, the alleviatory effect of *A. muciniphila* on ETEC K88 infection via the Wnt/β-catenin signaling pathway was confirmed with the addition of Wnt inhibitor Wnt-C59. The promoted proliferation and differentiation in the basal-out and apical-out intestinal organoids after co-culturing with *A. muciniphila* were reversed with Wnt-C59.

In conclusion, we found that FMT relieved intestinal inflammation and improved intestinal barrier function in AIMD piglets infected with ETEC K88. *A. muciniphila* was identified as key strain in FMT to promote the proliferation and differentiation of intestinal stem cells by mediating the Wnt/β catenin signaling pathway. The study revealed the possible mechanism that FMT alleviates the intestinal barrier injury.

DECLARATIONS

Ethics approval and Consent to participate

All animal experiments were performed according to the guidelines of the Animal Care Committee of Zhejiang University School of Medicine (permit number SYXK 2012-0178).

690 The animal care protocol was approved by the Local Committee of Animal Use following the
691 Guide for the Care and Use of Laboratory Animals (NIH publication 86-23 revised 1985).

692 **Consent for publication**

693 Not applicable.

694 **Availability of data and material**

695 The raw sequences derived from microbiome analysis for this study can be found in the
696 Sequence Read Archive (SRA) (https://www.ncbi.nlm.nih.gov/sra/PRJNA837047). And all
697 datasets analyzed in the present study are available from the corresponding author on
698 reasonable request.

699 **Competing interests**

700 The authors declared that the work was carried out in the absence of any commercial or
701 financial relationships that could be construed as a potential conflict of interest.

702 **Funding**

703 This research was supported by the National Natural Science Foundation of China (grant
704 number 32172765).

705 **Acknowledgments**

706 We appreciated the Experimental Teaching Center, College of Animal Science, Zhejiang
707 University for providing the AW400SG anaerobic workstations.

708

References

An DD, Oh SF, Olszak T, Neves JF, Avci FY, Erturk-Hasdemir D, Lu X, Zeissig S, Blumberg RS, Kasper DL. 2014. Sphingolipids from a Symbiotic Microbe Regulate Homeostasis of Host Intestinal Natural Killer T Cells. *Cell* **156**(1-2):123-133. DOI: https://doi.org/10.1016/j.cell.2013.11.042, PMID: 24439373.

Andremont A, Cervesi J, Bandinelli PA, Vitry F, de Gunzburg J. 2021. Spare and repair the gut microbiota from antibiotic-induced dysbiosis: state-of-the-art. *Drug Discovery Today* **26**(9):2159-2163. DOI: https://doi.org/10.1016/j.drudis.2021.02.022, PMID: 33639249.

Belzer C, de Vos WM. 2012. Microbes inside-from diversity to function: the case of *Akkermansia*. *ISME Journal* **6**(8):1449-1458. DOI: https://doi.org/10.1038/ismej.2012.6, PMID: 22437156.

Beumer J, Clevers H. 2021. Cell fate specification and differentiation in the adult mammalian intestine. *Nature Reviews Molecular Cell Biology* **22**(1):39-53. DOI: https://doi.org/10.1038/s41580-020-0278-0, PMID: 32958874.

Bian XY, Wu WR, Yang LY, Lv LX, Wang Q, Li YT, Ye JZ, Fang DQ, Wu JJ, Jiang XW, Shi D, Li LJ. 2019. Administration of *Akkermansia muciniphila* Ameliorates Dextran Sulfate Sodium-Induced Ulcerative Colitis in Mice. *Frontiers in Microbiology* **10**:2259. DOI: https://doi.org/10.3389/fmicb.2019.02259, PMID: 31632373.

Borody TJ, Eslick GD, Clancy RL. 2019. Fecal microbiota transplantation as a new therapy: from *Clostridioides difficile* infection to inflammatory bowel disease, irritable bowel syndrome, and colon cancer. *Current Opinion in Pharmacology* **49**:43-51. DOI: https://doi.org/10.1016/j.coph.2019.04.017, PMID: 31173991.

Buffie CG, Pamer EG. 2013. Microbiota-mediated colonization resistance against intestinal pathogens. *Nature Reviews Immunology* **13**(11):790-801. DOI: https://doi.org/10.1038/nri3535, PMID: 24096337.

Cammarota G, Ianiro G, Tilg H, Rajilic-Stojanovic M, Kump P, Satokari R, Sokol H, Arkkila P, Pintus C, Hart A, Segal J, Aloi M, Masucci L, Molinaro A, Scaldaferri F, Gasbarrini G, Lopez-Sanroman A, Link A, De Groot P, de Vos WM, Hoegenauer C, Malfertheiner P, Mattila E, Milosavljevic T, Nieuwdorp M, Sanguinetti M, Simren M, Gasbarrini A. 2017. European consensus conference on faecal microbiota transplantation in clinical practice. *Gut* **66**(4):569-580. DOI: https://doi.org/10.1136/gutjnl-2016-313017, PMID: 28087657.

Canfora EE, Meex RCR, Venema K, Blaak EE. 2019. Gut microbial metabolites in obesity, NAFLD and T2DM. *Nature Reviews Endocrinology* **15**(5):261-273. DOI: https://doi.org/10.1038/s41574-019-0156-z, PMID: 30670819.

Castro-Mejía J, Jakesevic M, Krych L, Nielsen DS, Hansen LH, Sondergaard BC, Kvist PH, Hansen AK, Holm TL. 2016. Treatment with a Monoclonal Anti-IL-12p40 Antibody Induces Substantial Gut Microbiota Changes in an Experimental Colitis Model. *Gastroenterology Research and Practice* **2016**:4953120. DOI: https://doi.org/10.1155/2016/4953120, PMID: 26880890.

Chelakkot C, Ghim J, Ryu SH. 2018. Mechanisms regulating intestinal barrier integrity and its pathological implications. *Experimental & Molecular Medicine* **50**(8):1-9. DOI: https://doi.org/10.1038/s12276-018-0126-x, PMID: 30115904.

Co JY, Margalef-Català M, Monack DM, Amieva MR. 2021. Controlling the polarity of human gastrointestinal organoids to investigate epithelial biology and infectious diseases. *Nature Protocols* **16**(11):5171-5192. DOI: https://doi.org/10.1038/s41596-021-00607-0, PMID: 34663962.

Co JY, Margalef-Català M, Li XN, Mah AT, Kuo CJ, Monack DM, Amieva MR. 2019. Controlling Epithelial Polarity: A Human Enteroid Model for Host-Pathogen Interactions. *Cell Reports* **26**(9):2509-2520. DOI: https://doi.org/10.1016/j.celrep.2019.01.108, PMID: 30811997.

Colman RJ, Rubin DT. 2014. Fecal microbiota transplantation as therapy for inflammatory bowel disease: A systematic review and meta-analysis. *Journal of Crohns & Colitis* **8**(12):1569-1581. DOI: https://doi.org/10.1016/j.crohns.2014.08.006, PMID: 25223604.

Deng HM, Li ZC, Tan YF, Guo ZB, Liu YY, Wang Y, Yuan Y, Yang RF, Bi YJ, Bai Y, Zhi FC. 2016. A novel strain of *Bacteroides fragilis* enhances phagocytosis and polarises M1 macrophages. *Scientific Reports* **6**:29401. DOI: https://doi.org/10.1038/srep29401, PMID: 27381366.

Donaldson GP, Lee SM, Mazmanian SK. 2016. Gut biogeography of the bacterial microbiota. *Nature Reviews Microbiology* **14**(1):20-32. DOI: https://doi.org/10.1038/nrmicro3552, PMID: 26499895.

Dubreuil JD. 2021. Pig vaccination strategies based on enterotoxigenic *Escherichia coli* toxins. *Brazilian Journal of Microbiology* **52**(4):2499-2509. DOI: https://doi.org/10.1007/s42770-021-00567-3, PMID: 34244980.

Everard A, Belzer C, Geurts L, Ouwerkerk JP, Druart C, Bindels LB, Guiot Y, Derrien M, Muccioli GG, Delzenne NM, de Vos WM, Cani PD. 2013. Cross-talk between *Akkermansia muciniphila* and intestinal epithelium controls diet-induced obesity. *Proceedings of the National Academy of Sciences of the United States of America* **110**(22):9066-9071. DOI: https://doi.org/10.1073/pnas.1219451110, PMID: 23671105.

Flint H, Scott KP, Louis P, Duncan SH. 2012. The role of the gut microbiota in nutrition and health. *Nature Reviews Gastroenterology & Hepatology* **9**(10):577-589. DOI: https://doi.org/10.1038/nrgastro.2012.156, PMID: 22945443.

Francino MP. 2016. Antibiotics and the Human Gut Microbiome: Dysbioses and Accumulation of Resistances. *Frontiers in Microbiology* **6**:1543. DOI: https://doi.org/10.3389/fmicb.2015.01543, PMID: 26793178.

Geng SJ, Cheng SS, Li Y, Wen ZS, Ma X, Jiang XM, Wang YZ, Han XY. 2018. Faecal Microbiota Transplantation Reduces Susceptibility to Epithelial Injury and Modulates Tryptophan Metabolism of the Microbial Community in a Piglet Model. *Journal of Crohns & Colitis* **12**(11):1359-1374. DOI: https://doi.org/10.1093/ecco-jcc/jjy103, PMID: 30010734.

Ghosh S, Whitley CS, Haribabu B, Jala VR. 2021. Regulation of Intestinal Barrier Function by Microbial Metabolites. *Cellular and Molecular Gastroenterology and Hepatology* **11**(5):1464-1482. DOI: https://doi.org/10.1016/j.jcmgh.2021.02.007, PMID: 33610769.

Hou QH, Dong YY, Yu QH, Wang B, Le S, Guo YM, Zhang BK. 2020. Regulation of the Paneth cell niche by exogenousL-arginine couples the intestinal stem cell function. *FASEB Journal* **34**(8): 10299-10315. DOI: https://doi.org/10.1096/fj.201902573RR, PMID: 32725957.

Hsiao EY, McBride SW, Hsien S, Sharon G, Hyde ER, McCue T, Codelli JA, Chow J, Reisman SE, Petrosino JF, Patterson PH, Mazmanian SK. 2013. Microbiota Modulate Behavioral and Physiological Abnormalities Associated with Neurodevelopmental Disorders. *Cell* **155**(7):1451-1463. DOI: https://doi.org/10.1016/j.cell.2013.11.024, PMID: 24315484.

Li J, Lin SQ, Vanhoutte PM, Woo CW, Xu AM. 2016. *Akkermansia Muciniphila* Protects Against Atherosclerosis by Preventing Metabolic Endotoxemia-Induced Inflammation in Apoe$^{-/-}$ Mice. *Circulation* **133**(24):2423-2446. DOI: https://doi.org/10.1161/CIRCULATIONAHA.115.019645, PMID: 27143680.

Li Y, Yang N, Chen JN, Huang X, Zhang N, Yang SS, Liu G, Liu GL. 2020. Next-Generation Porcine Intestinal Organoids: an Apical-Out Organoid Model for Swine Enteric Virus Infection and Immune Response Investigations. *Journal of Virology* **94**(21):e01006-20. DOI: https://doi.org/10.1128/JVI.01006-20, PMID: 32796075.

Luo HM, Li MX, Wang F, Yang YF, Wang Q, Zhao YS, Du FK, Chen Y, Shen J, Zhao QY, Zeng JP, Wang SP, Chen MJ, Li XB, Li WP, Sun YH, Gu L, Wen QL, Xiao ZG, Wu X. 2022. The role of intestinal stem cell within gut homeostasis: Focusing on its interplay with gut microbiota and the regulating pathways. *International Journal of Biological Sciences* **18**(13):5185-5206. DOI: https://doi.org/10.7150/ijbs.72600, PMID: 35982910.

Luo QW, Kumar P, Vickers TJ, Sheikh A, Lewis WG, Rasko DA, Sistrunk J, Fleckenstein JM. 2014. Enterotoxigenic Escherichia coli Secretes a Highly Conserved Mucin-Degrading Metalloprotease To Effectively Engage Intestinal Epithelial Cells. *Infection and Immunity* **82**(2):509-521. DOI: https://doi.org/10.1128/IAI.01106-13, PMID: 24478067.

Ma X, Xu TT, Qian MQ, Zhang YC, Yang ZR, Han XY. 2021. Faecal microbiota transplantation alleviates early-life antibiotic-induced gut microbiota dysbiosis and mucosa injuries in a neonatal piglet model. *Microbiological Research* **255**:126942. DOI: https://doi.org/10.1016/j.micres.2021.126942, PMID: 34915267.

Nash TJ, Morris KM, Mabbott NA, Vervelde L. 2021. Inside-out chicken enteroids with leukocyte component as a model to study host-pathogen interactions. *Communications Biology* **4**(1):377. DOI: https://doi.org/10.1038/s42003-021-01901-z, PMID: 33742093.

Nguyen LH, Örtqvist AK, Cao Y, Simon TG, Roelstraete B, Song MY, Joshi AD, Staller K, Chan AT, Khalili H, Olén O, Ludvigsson JF. 2020. Antibiotic use and the development of inflammatory bowel disease: a national case-control study in Sweden. *Lancet Gastroenterology & Hepatology* **5**(11):986-995. DOI: https://doi.org/10.1016/S2468-1253(20)30267-3, PMID: 32818437.

Niehrs C. 2012. The complex world of WNT receptor signaling. *Nature Reviews Molecular Cell Biology* **13**(12):767-779. DOI: https://doi.org/10.1038/nrm3470, PMID: 23151663.

Ottman N, Reunanen J, Meijerink M, Pietilä TE, Kainulainen V, Klievink J, Huuskonen L, Aalvink S, Skurnik M, Boeren S, Satokari R, Mercenier A, Palva A, Smidt H, de Vos WM, Belzer C. 2017. Pili-like proteins of *Akkermansia muciniphila* modulate host immune responses and gut barrier function. *PLoS One* **12**(3):e0173004. DOI: https://doi.org/10.1371/journal.pone.0173004, PMID: 28249045.

Plovier H, Everard A, Druart C, Depommier C, Van Hul M, Geurts L, Chilloux J, Ottman N, Duparc T, Lichtenstein L, Myridakis A, Delzenne NM, Klievink J, Bhattacharjee A, van der Ark KCH, Aalvink S, Martinez LO, Dumas ME, Maiter D, Loumaye A, Hermans MP, Thissen JP, Belzer C, de Vos WM, Cani PD. 2017. A purified membrane protein from *Akkermansia muciniphila* or the pasteurized bacterium improves metabolism in obese and diabetic mice. *Nature Medicine* **23**(1):107-113. DOI: https://doi.org/10.1038/nm.4236, PMID: 27892954.

Quraishi MN, Widlak M, Bhala N, Moore D, Price M, Sharma N, Iqbal TH. 2017. Systematic review with meta-analysis: the efficacy of faecal microbiota transplantation for the treatment of recurrent and refractory *Clostridium difficile* infection. *Alimentary Pharmacology & Therapeutics* **46**(5):479-493. DOI: https://doi.org/10.1111/apt.14201, PMID: 28707337.

Ring A, Kim YM, Kahn M. 2014. Wnt/Catenin Signaling in Adult Stem Cell Physiology and Disease. *Stem Cell Reviews and Reports* **10**(4):512-525. DOI: https://doi.org/10.1007/s12015-014-9515-2, PMID: 24825509.

Sato T, Vries RG, Snippert HJ, van de Wetering M, Barker N, Stange DE, van Es JH, Abo A, Kujala P, Peters PJ, Clevers H. 2009. Single Lgr5 stem cells build crypt-villus structures *in vitro* without a mesenchymal niche. *Nature* **459**(7244):262-U147. DOI: https://doi.org/10.1038/nature07935, PMID: 19329995.

Shi Y, Shu B, Yang RH, Xu YB, Xing BR, Liu J, Chen L, Qi SH, Liu XS, Wang P, Tang JM, Xie JL. 2015. Wnt and Notch signaling pathway involved in wound healing by targeting *c-Myc* and *Hes1* separately. *Stem Cell Research & Therapy* **6**:120. DOI: https://doi.org/10.1186/s13287-015-0103-4, PMID: 26076648/

Smith D, Price DRG, Burrells A, Faber MN, Hildersley KA, Chintoan-Uta C, Chapuis AF, Stevens M, Stevenson K, Burgess STG, Innes EA, Nisbet AJ, McNeilly TN. 2021. The Development of Ovine Gastric and Intestinal Organoids for Studying Ruminant Host-Pathogen Interactions. *Frontiers in Cellular and Infection Microbiology* **11**:733811. DOI: https://doi.org/10.3389/fcimb.2021.733811, PMID: 34568096.

Sprangers J, Zaalberg IC, Maurice MM. 2021. Organoid-based modeling of intestinal development, regeneration, and repair. *Cell Death and Differentiation* **28**(1):95-107. DOI: https://doi.org/10.1038/s41418-020-00665-z, PMID: 33208888.

Sun FT, Zhang QS, Zhao JX, Zhang H, Zhai QX, Chen W. 2019. A potential species of next-generation probiotics? The dark and light sides of Bacteroides fragilis in health. *Food Research International* **126**:108590. DOI: https://doi.org/10.1016/j.foodres.2019.108590, PMID: 31732047.

Sun YW, Kim SW. 2017. Intestinal challenge with enterotoxigenic *Escherichia coli* in pigs, and nutritional intervention to prevent postweaning diarrhea. *Animal Nutrition* **3**(4):322-330. DOI: https://doi.org/10.1016/j.aninu.2017.10.001, PMID: 29767133.

Troy EB, Kasper DL.2010. Beneficial effects of Bacteroides fragilis polysaccharides on the immune system. *Frontiers in Bioscience-Landmark* **15**:25-34. DOI: https://doi.org/10.2741/3603, PMID: 20036803.

Wang C, Li SJ, Hong K, Yu LL, Tian FW, Zhao JX, Zhang H, Chen W, Zhai QX. 2021. The roles of different *Bacteroides fragilis* strains in protecting against DSS-induced ulcerative colitis and related functional genes. *Food & Function* **12**(18):8300-8313. DOI: https://doi.org/10.1039/d1fo00875g, PMID: 34308455.

Wang WW, Wang Y, Hao XR, Duan YX, Meng ZQ, An XP, Qi JW. 2020. Dietary fermented soybean meal replacement alleviates diarrhea in weaned piglets challenged with enterotoxigenic *Escherichia coli* K88 by modulating inflammatory cytokine levels and cecal microbiota composition. *BMC Veterinary Research* **16**(1):245. DOI: https://doi.org/10.1186/s12917-020-02466-5, PMID: 32664940.

Witkowski M,Weeks TL, Hazen SL. 2020. Gut Microbiota and Cardiovascular Disease. *Circulation Research* **127**(4):553-570. DOI: https://doi.org/10.1161/CIRCRESAHA.120.316242, PMID: 32762536.

Wlodarska M, Willing B, Keeney KM, Menendez A, Bergstrom KS, Gill N, Russell SL, Vallance BA, Finlay BB. 2011. *Infection and Immunity* **79**(4):1536-1545. DOI: https://doi.org/10.1128/IAI.01104-10, PMID: 21321077.

Xie WC, Song LY, Wang XY, Xu YG, Liu ZS, Zhao DF, Wang SB, Fan XL, Wang ZR, Gao C, Wang XN, Wang L, Qiao XY, Zhou H, Cui W, Jiang YP, Li YJ, Tang LJ. 2021. A bovine lactoferricin-lactoferrampin-encoding Lactobacillus reuteri CO21 regulates the intestinal mucosal immunity and enhances the protection of piglets against enterotoxigenic *Escherichia coli* K88 challenge. *Gut Microbes* **13**(1):1956281. DOI: https://doi.org/10.1080/19490976.2021.1956281, PMID: 34369287.

878 **Yan** KS, Janda CY, Chang JL, Zheng GXY, Larkin KA, Luca VC, Chia LA, Mah AT, Han A, Terry JM,
879 Ootani A, Roelf K, Lee M, Yuan J, Li X, Bolen CR, Wilhelmy J, Davies PS, Ueno H, von Furstenberg RJ,
880 Belgrader P, Ziraldo SB, Ordonez H, Henning SJ, Wong MH, Snyder MP, Weissman IL, Hsueh AJ,
881 Mikkelsen TS, Garcia KC, Kuo CJ. 2017. Non-equivalence of Wnt and R-spondin ligands during $Lgr5^{+}$
882 intestinal stem-cell self-renewal. *Nature* **545**(7653):238-242. DOI: https://doi.org/10.1038/nature22313,
883 PMID: 28467820.
884 **Yin** YB, Guo SG, Wan D, Wu X, Yin YL. 2019. Enteroids: Promising in Vitro Models for Studies of
885 Intestinal Physiology and Nutrition in Farm Animals. *Journal of Agricultural and Food Chemistry*
886 **67**(9):2421-2428. DOI: https://doi.org/10.1021/acs.jafc.8b06908, PMID: 30739438.
887 **Yu** HT, Ding XL, Shang LJ, Zeng XF, Liu HB, Li N, Huang S, Wang YM, Wang G, Cai S, Chen MX,
888 Levesque CL, Johnston LJ, Qiao SY. 2018. Protective Ability of Biogenic Antimicrobial Peptide
889 Microcin J25 Against Enterotoxigenic Escherichia Coli-Induced Intestinal Epithelial Dysfunction and
890 Inflammatory Responses IPEC-J2 Cells. *Frontiers in Cellular and Infection Microbiology* **8**:242. DOI:
891 https://doi.org/10.3389/fcimb.2018.00242, PMID: 30057893.
892 **Zhai R**, Xue XH, Zhang LY, Yang X, Zhao LP, Zhang CH. 2019. Strain-Specific Anti-inflammatory
893 Properties of Two *Akkermansia muciniphila* Strains on Chronic Colitis in Mice. *Frontiers in Cellular*
894 *and Infection Microbiology* **9**:239. DOI: https://doi.org/10.3389/fcimb.2019.00239, PMID: 31334133.
895 **Zhang L**, Qin QQ, Liu MN, Zhang XL, He F, Wang GQ. 2018. *Akkermansia muciniphila* can reduce the
896 damage of gluco/lipotoxicity, oxidative stress and inflammation, and normalize intestine microbiota in
897 streptozotocin-induced diabetic rats. *Pathogens and Disease* **76**(4):fty028. DOI:
898 https://doi.org/10.1093/femspd/fty028, PMID: 29668928.
899 **Zheng SY**, Li HX, Xu RC, Miao WT, Dai MY, Ding ST, Liu HD. 2021. Potential roles of gut microbiota
900 and microbial metabolites in Parkinson's disease. *Ageing Research Reviews* **69**:101347. DOI:
901 https://doi.org/10.1016/j.arr.2021.101347, PMID: 33905953.
902 **Zheng Y**, Wang L, Zhang JP, Yang JY, Zhao ZM, Zhang XY. 2010. Expression of p53, c-erbB-2 and Ki67
903 in intestinal metaplasia and gastric carcinoma. *World Journal of Gastroenterology* **16**(3):339-344. DOI:
904 https://doi.org/10.3748/wjg.v16.i3.339, PMID: 20082479.
905 **Zhou JY**, Huang DG, Gao CQ, Yan HC, Zou SG, Wang XQ. 2021. Heat-stable enterotoxin inhibits
906 intestinal stem cell expansion to disrupt the intestinal integrity by downregulating the Wnt/β-catenin
907 pathway. *Stem Cell* **39**(4):482-496. DOI: https://doi.org/10.1002/stem.3324, PMID: 33373490.
908 **Zhu LD**, Lu XX, Liu L, Voglmeir J, Zhong X, Yu QH. 2020. *Akkermansia muciniphila* protects intestinal
909 mucosa from damage caused by *S. pullorum* by initiating proliferation of intestinal epithelium.
910 *Veterinary Research* **51**(1):34. DOI: https://doi.org/10.1186/s13567-020-00755-3, PMID: 32138776.
911
912

Figure legends:

Figure 1. Experimental designs of the present study. (A) Schematic diagram of the FMT administered to the AIMD piglets infected with ETEC K88. (B) Schematic diagram of the alleviatory effects of *A. muciniphila* and *B. fragilis* on ETEC K88 infection in mice. (C) Schematic diagram of the alleviatory effects of *A. muciniphila* on ETEC K88 infection in porcine basal-out and apical-out intestinal organoids.

Figure 2. FMT improved the growth performance and inflammatory response of AIMD piglets infected with ETEC K88. (A) Average daily weight gain (ADG) in the Con, EP and EF groups. (B) Diarrhea score at days 3 and 6 post-infection. (C) The colonization of ETEC K88 in the jejunum and colon. The melting curve demonstrated that only the ETEC K88 could be amplified by the primers we used. (D) The relative mRNA expression of cytokines in the jejunum. Con: control group, EP: ETEC K88 + PBS group, EF: ETEC K88 + FMT group. Data are expressed as the mean ± SD. *, $P < 0.05$, **, $P < 0.01$, ***, $P < 0.001$.

Figure 3. FMT improved the intestinal morphology and barrier function in AIMD piglets infected with ETEC K88. (A) SEM images of villi (top) and microvilli (bottom) in the jejunum (scale bars = 300 or 2 μm). (B) The relative mRNA expression of tight junction proteins (ZO-1, claudin and occludin) and adheren junctions (β-catenin and E-cadherin) in the jejunum. (C) The relative protein expression of tight junction proteins (ZO-1, claudin and occludin) and adheren junction proteins (β-catenin and E-cadherin) in the jejunum. (D) Immunofluorescence images of Mucin 2 (MUC2, green) in the jejunum (scale bars = 50 μm). Con: control group, EP: ETEC K88 + PBS group, EF: ETEC K88 + FMT group. Data are expressed as the mean ± SD. *, $P < 0.05$, **, $P < 0.01$. Data shown are representative of at least two independent experiments.

Figure 4. FMT changed the composition of gut microbiota and the concentration of SCFAs in AIMD piglets infected with ETEC K88. (A) Anosim analysis. (B) UPGMA clustering analysis based on Unweighted unifrac distance. (C) LEfSe analysis with LDA score > 4. (D) Quantification of SCFA metabolites (acetic acid, propionic acid, butyric acid, isobutyric acid, isovaleric acid and hexanoic acid). EP: ETEC K88 + PBS group, EF: ETEC K88 + FMT group. Data are expressed as the mean ± SD. *, $P < 0.05$, **, $P < 0.01$. Data shown are representative of at least two independent experiments.

Figrue 5. *A. muciniphila* and *B. fragilis* improved the intestinal morphology of mice infected with ETEC K88. (A) H&E-stained images of jejunum (scale bars = 50 μm) and the histograms of villus height, crypt depth and the ratio of villus height to crypt depth. (B) TEM images of jejunum and colon (scale bars = 0.5 μm). (C) Immunofluorescence images of Mucin 2 (MUC2, green) in the jejunum and colon (scale bars = 50 μm). C: control group, E: ETEC K88 + PBS group, A: ETEC K88 + *A. muciniphila* group, B: ETEC K88 + *B. fragilis* group. Data are expressed as the mean ± SD. *, $P < 0.05$, **, $P < 0.01$, ***, $P < 0.001$. Data shown are representative of at least two independent experiments.

Figure 6. *A. muciniphila* and *B. fragilis* regulated the expression of inflammatory cytokines and the balance of Treg and Th17 cells in mice infected with ETEC K88. (A) The relative mRNA expression of cytokines in the jejunum. (B) Flow cytometric dot plots and proportions of Treg ($CD25^+Foxp3^+$), Th17 ($CD4^+ROR\gamma t^+$) and mature dendritic cells ($CD86^+CD11C^+$) in jejunal lamina propria. C: control group, E: ETEC K88 + PBS group, A: ETEC K88 + *A. muciniphila* group, B: ETEC K88 + *B. fragilis* group. Data are expressed as the mean ± SD. *, $P < 0.05$, **, $P < 0.01$, ***, $P < 0.001$. Data shown are representative of at least two independent experiments.

Figure 7. *A. muciniphila* and *B. fragilis* enhanced the number of Ki67 cells and Lyz Paneth cells in jejunal crypt of mice infected with ETEC K88 by moderately activating the Wnt/β-catenin pathway.

(A) The mRNA expression and immunofluorescence staining images of intestinal epithelial cell proliferation marker Ki67 (red). (B) The mRNA expression and immunofluorescence staining images of Paneth marker Lyz (green). (C) The relative mRNA expression of *Lgr5*, *Wnt3*, *Notch1* and other genes in jejunum mucosa. (D) The relative protein expression of Wnt/β-catenin pathway and its target genes in jejunum mucosa. C: control group, E: ETEC K88 + PBS group, A: ETEC K88 + *A. muciniphila* group, B: ETEC K88 + *B. fragilis* group. Data are expressed as the mean ± SD. *, $P < 0.05$, **, $P < 0.01$, ***, $P < 0.001$. Data shown are representative of at least two independent experiments.

Figure 8. *A. muciniphila* and *B. fragilis* promoted the activity of Lgr5$^+$ intestinal stem cells as proved by the growth of intestinal organoids. (A) Morphology of *ex vivo* culture of crypts isolated from the jejunum of mice in the C, E, A and B groups (Day 5; 4 ×, scale bars = 200 μm; 20 ×, scale bars = 50 μm). (B) The surface area and forming efficiency of intestinal organoids. (C) The relative mRNA expression of genes related to the proliferation and differentiation of the intestinal organoids. C: control group, E: ETEC K88 + PBS group, A: ETEC K88 + *A. muciniphila* group, B: ETEC K88 + *B. fragilis* group. Data are expressed as the mean ± SD. *, $P < 0.05$, **, $P < 0.01$, ***, $P < 0.001$. Data shown are representative of at least two independent experiments.

Figure 9. *A. muciniphila* protected the Lgr5$^+$ intestinal stem cell and activated the Wnt/β-catenin signaling pathway of the ETEC K88-induced basal-out intestinal organoids. (A) The relative mRNA expression of *villin*, *ZO-1*, *Ki67*, *Lyz1*, *MUC2*, *Lgr5*, *Wnt3a* and *β-catenin* genes. (B)-(F) Immunofluorescence images of villin (scale bars = 50 μm), Ki67 (scale bars = 50 μm), Lgr5 (scale bars = 20 μm), Wnt3a (scale bars = 50 μm) and β-catenin (scale bars = 50 μm). (G) Fold change of the mean fluorescence intensity. CON: control group, ETEC: ETEC K88 + DMEM/F-12 group, AKK: ETEC K88 + *A. muciniphila* group, WNT-C59: Wnt-C59 + ETEC K88 + *A. muciniphila* group. Data are expressed as the mean ± SD. *, $P < 0.05$, **, $P < 0.01$, ***, $P < 0.001$. Data shown are representative of at least two independent experiments.

Figure 10. *A. muciniphila* alleviated the intestinal epithelial injury of the ETEC K88-induced apical-out intestinal organoids. (A) Confocal microscope visualization of the apical-out intestinal organoids incubated in FD4 solution (scale bars = 50 μm). (B) The relative mRNA expression of *villin*, *ZO-1*, *Ki67*, *Lyz1*, *MUC2*, *Lgr5*, *Wnt3a* and *β-catenin* genes. (C)-(G) Immunofluorescence images of villin, Ki67, Lgr5, Wnt3a and β-catenin (scale bars = 20 μm). (H) Quantification of the apical-out intestinal organoids incubated in FD4 solution that have intact barrier integrity. (I) Fold change of the mean fluorescence intensity. (J) The relative mRNA expression of cytokines in the apical-out intestinal organoids. CON: control group, ETEC: ETEC K88 + DMEM/F-12 group, AKK: ETEC K88 + *A. muciniphila* group, WNT-C59: Wnt-C59 + ETEC K88 + *A. muciniphila* group. Data are expressed as the mean ± SD. *, $P < 0.05$, **, $P < 0.01$, ***, $P < 0.001$. Data shown are representative of at least two independent experiments.

991

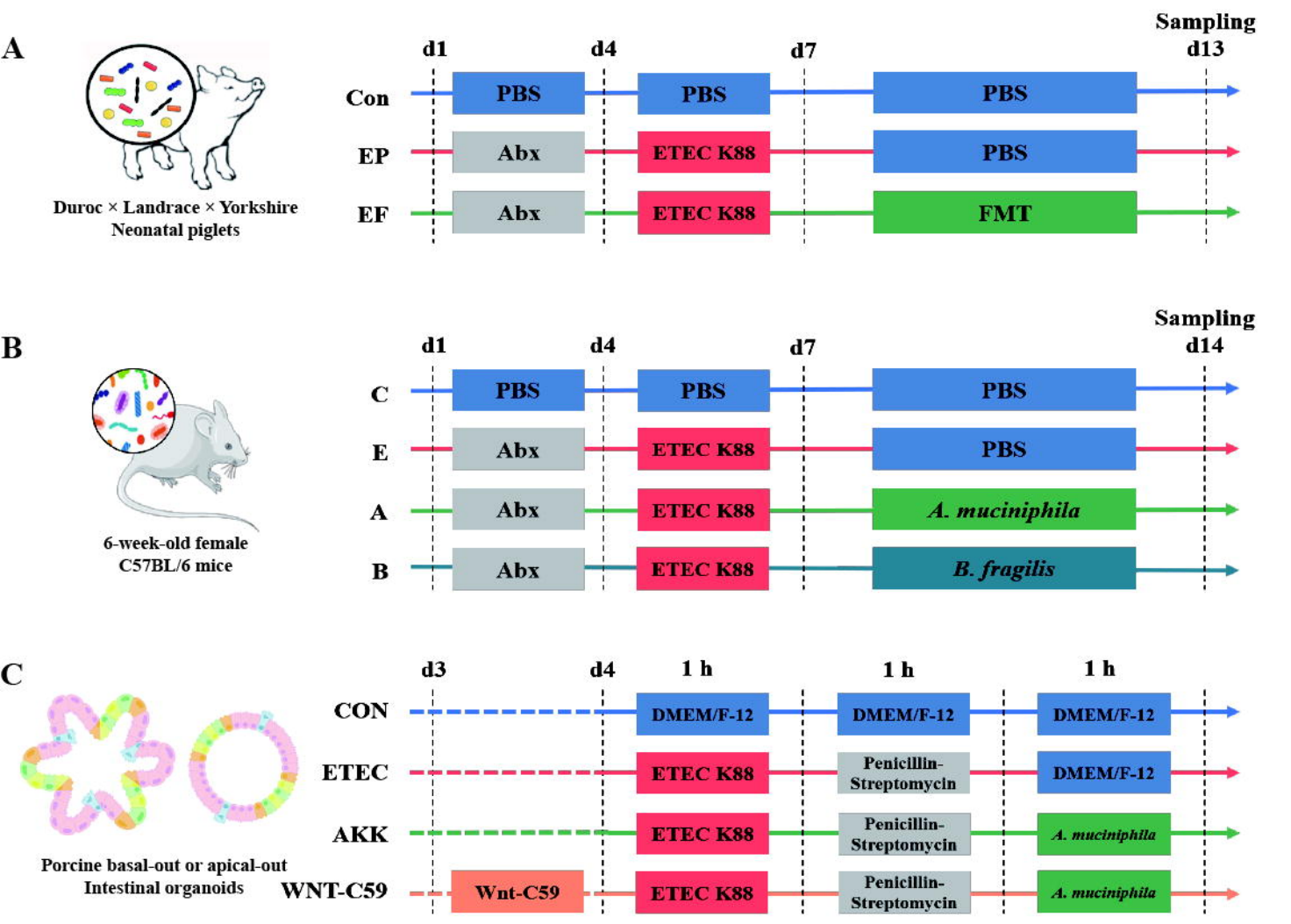
A
Duroc × Landrace × Yorkshire
Neonatal piglets
d1
d4
d7
Sampling
d13
Con
EP
EF
PBS
PBS
PBS
Abx
ETEC K88
PBS
Abx
ETEC K88
FMT
B
6-week-old female
C57BL/6 mice
d1
d4
d7
Sampling
d14
C
E
A
B
PBS
PBS
PBS
Abx
ETEC K88
PBS
Abx
ETEC K88
A. muciniphila
Abx
ETEC K88
B. fragilis
C
Porcine basal-out or apical-out
Intestinal organoids
d3
d4
1 h
1 h
1 h
CON
ETEC
AKK
WNT-C59
DMEM/F-12
DMEM/F-12
DMEM/F-12
ETEC K88
Penicillin-Streptomycin
DMEM/F-12
ETEC K88
Penicillin-Streptomycin
A. muciniphila
Wnt-C59
ETEC K88
Penicillin-Streptomycin
A. muciniphila

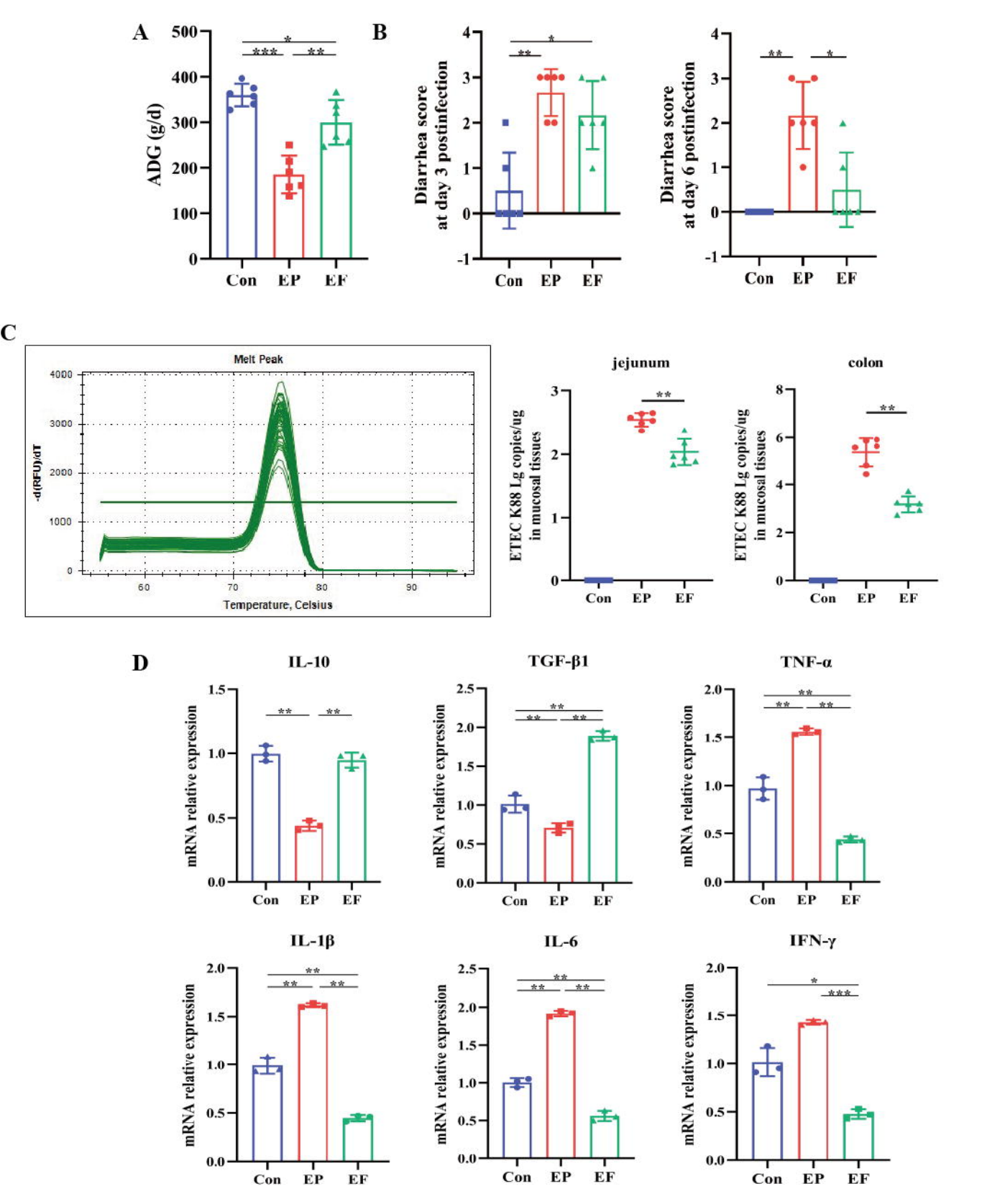
A
ADG (g/d)
Con
EP
EF
B
Diarrhea score at day 3 postinfection
Diarrhea score at day 6 postinfection
C
Melt Peak
-d(RFU)/dT
Temperature, Celsius
jejunum
colon
ETEC K88 Lg copies/ug in mucosal tissues
D
IL-10
TGF-β1
TNF-α
IL-1β
IL-6
IFN-γ
mRNA relative expression

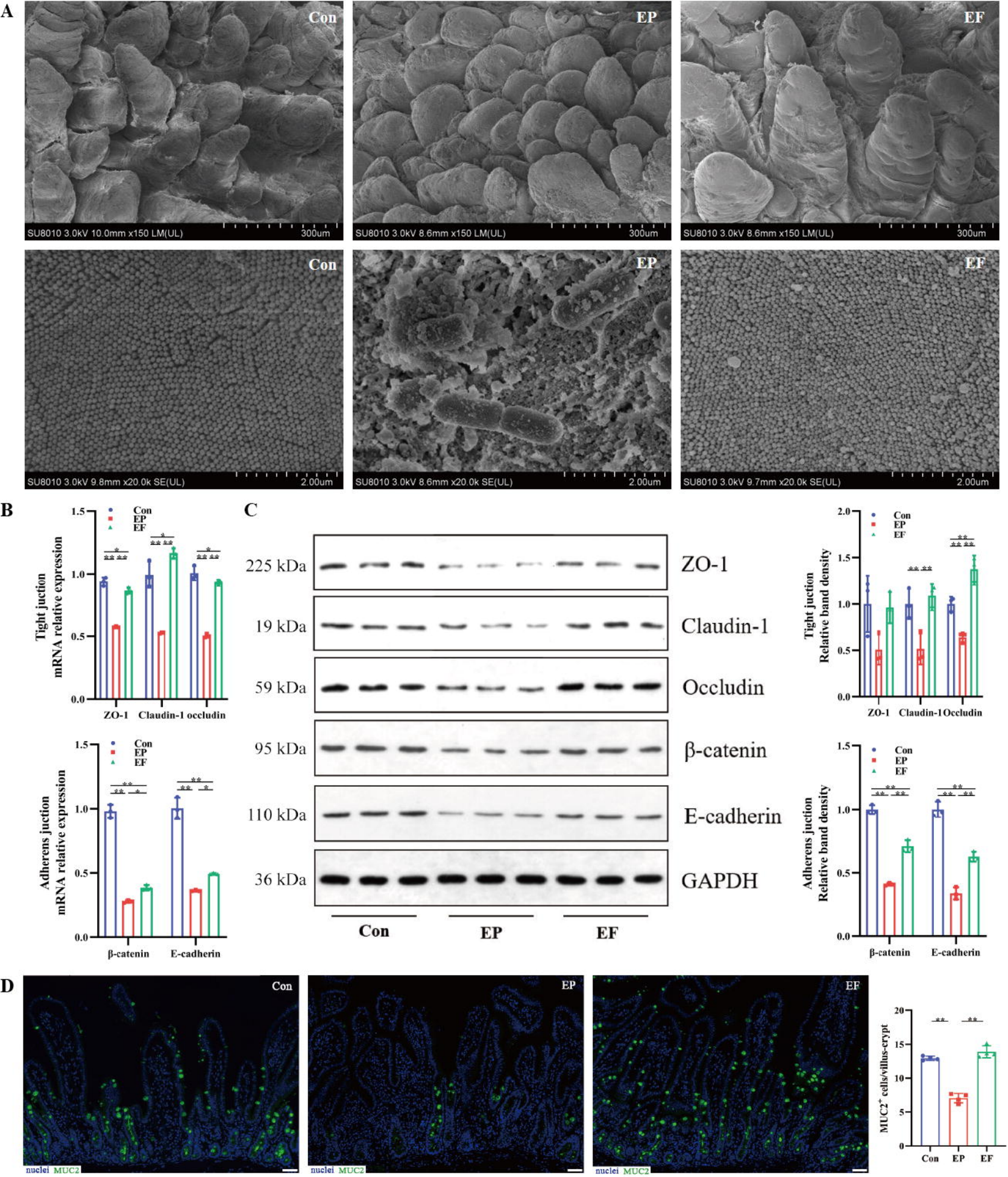
A
Con
EP
EF
SU8010 3.0kV 10.0mm x150 LM(UL)
300um
SU8010 3.0kV 8.6mm x150 LM(UL)
300um
SU8010 3.0kV 8.6mm x150 LM(UL)
300um
SU8010 3.0kV 9.8mm x20.0k SE(UL)
2.00um
SU8010 3.0kV 8.6mm x20.0k SE(UL)
2.00um
SU8010 3.0kV 9.7mm x20.0k SE(UL)
2.00um
B
Tight junction mRNA relative expression
ZO-1
Claudin-1
occludin
Adherens junction mRNA relative expression
β-catenin
E-cadherin
C
225 kDa
ZO-1
19 kDa
Claudin-1
59 kDa
Occludin
95 kDa
β-catenin
110 kDa
E-cadherin
36 kDa
GAPDH
Con
EP
EF
Tight junction Relative band density
Adherens junction Relative band density
D
nuclei MUC2
MUC2+ cells/villus-crypt

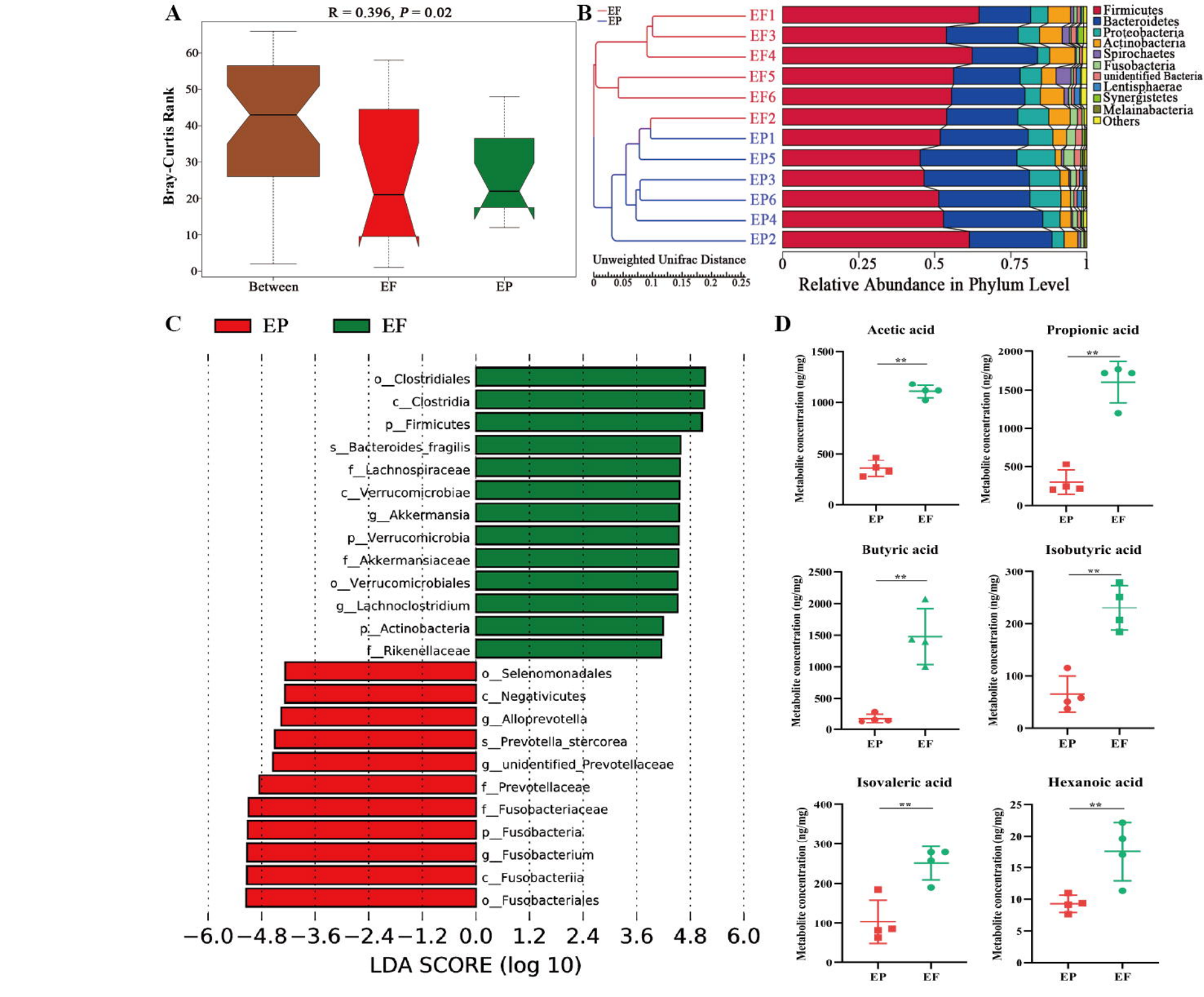
A
R = 0.396, P = 0.02
Bray-Curtis Rank
Between
EF
EP
B
EF
EP
EF1
EF3
EF4
EF5
EF6
EF2
EP1
EP5
EP3
EP6
EP4
EP2
Unweighted Unifrac Distance
Relative Abundance in Phylum Level
Firmicutes
Bacteroidetes
Proteobacteria
Actinobacteria
Spirochaetes
Fusobacteria
unidentified Bacteria
Lentisphaerae
Synergistetes
Melainabacteria
Others
C
EP
EF
o__Clostridiales
c__Clostridia
p__Firmicutes
s__Bacteroides_fragilis
f__Lachnospiraceae
c__Verrucomicrobiae
g__Akkermansia
p__Verrucomicrobia
f__Akkermansiaceae
o__Verrucomicrobiales
g__Lachnoclostridium
p__Actinobacteria
f__Rikenellaceae
o__Selenomonadales
c__Negativicutes
g__Alloprevotella
s__Prevotella_stercorea
g__unidentified_Prevotellaceae
f__Prevotellaceae
f__Fusobacteriaceae
p__Fusobacteria
g__Fusobacterium
c__Fusobacteriia
o__Fusobacteriales
LDA SCORE (log 10)
D
Acetic acid
Propionic acid
Butyric acid
Isobutyric acid
Isovaleric acid
Hexanoic acid
Metabolite concentration (ng/mg)
EP
EF

A

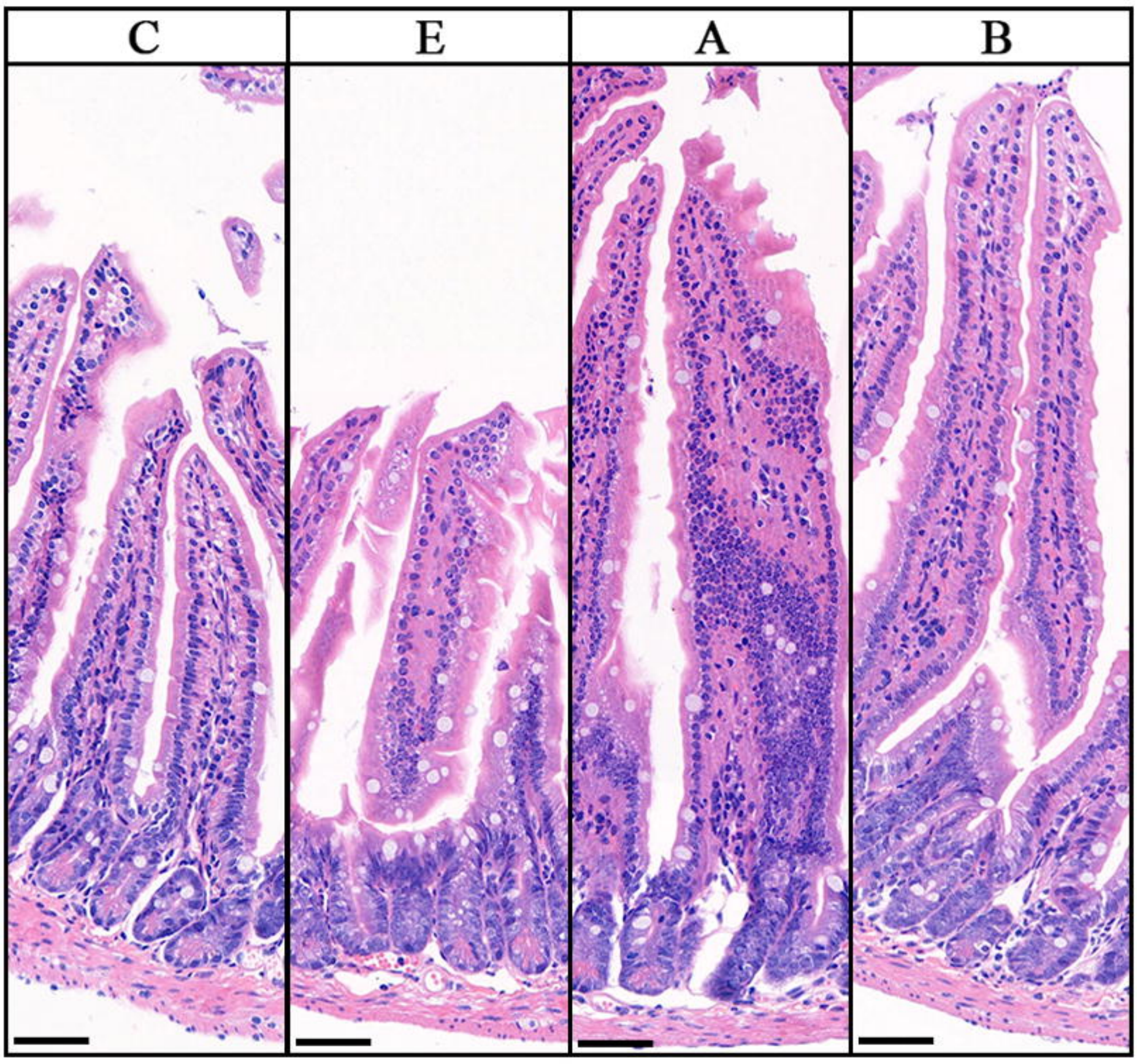

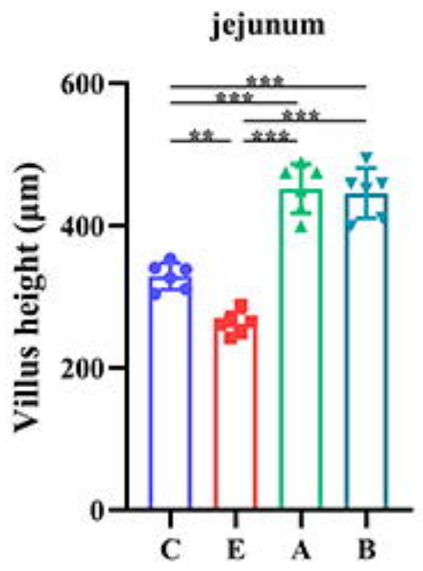

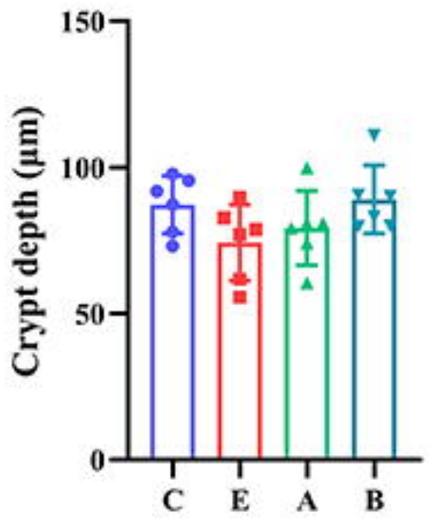

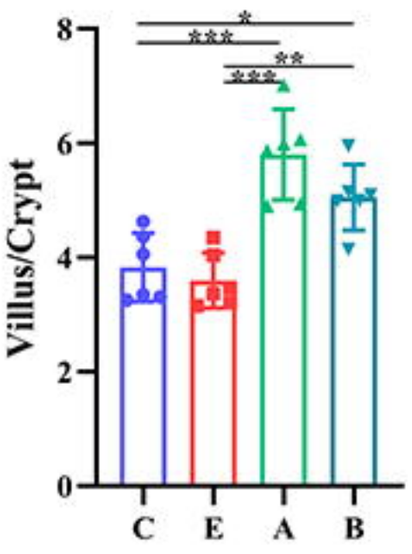

B

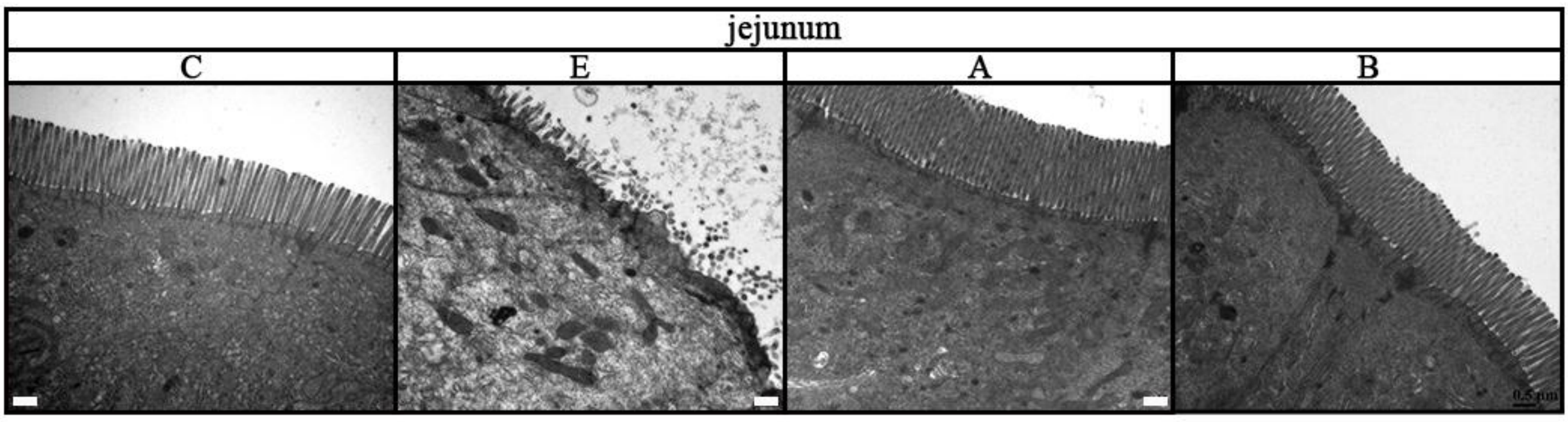

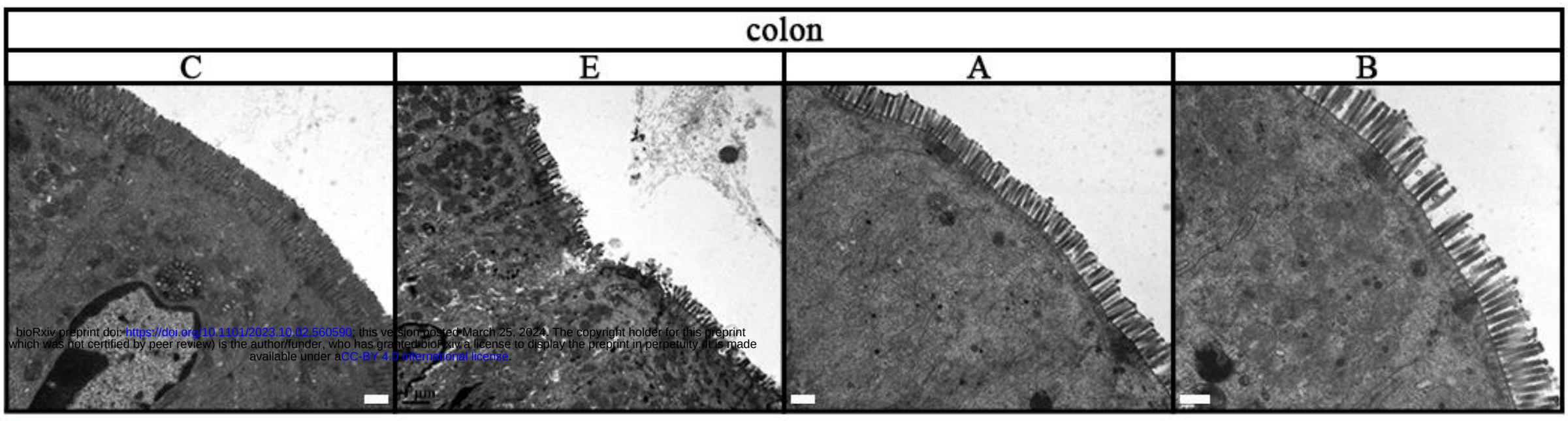

C

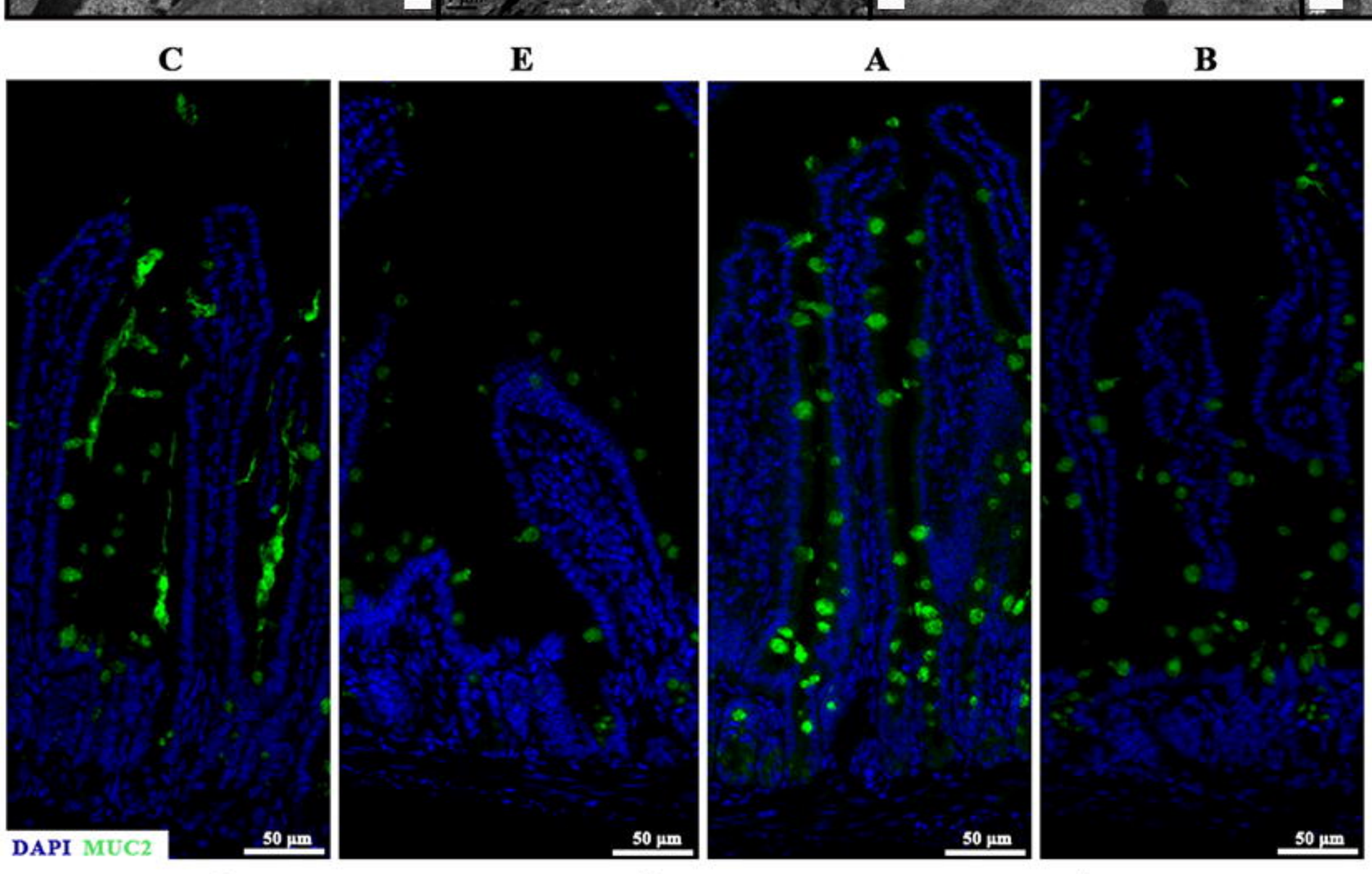

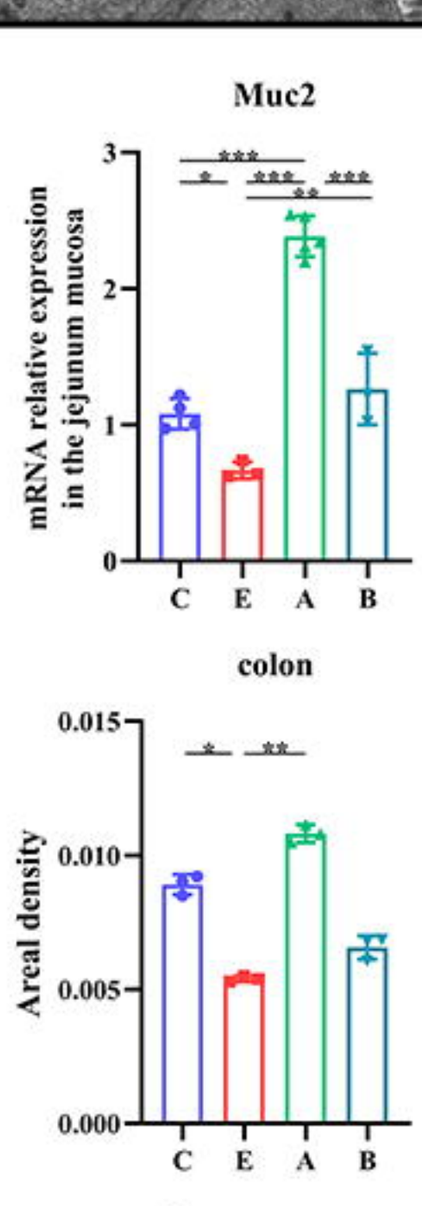

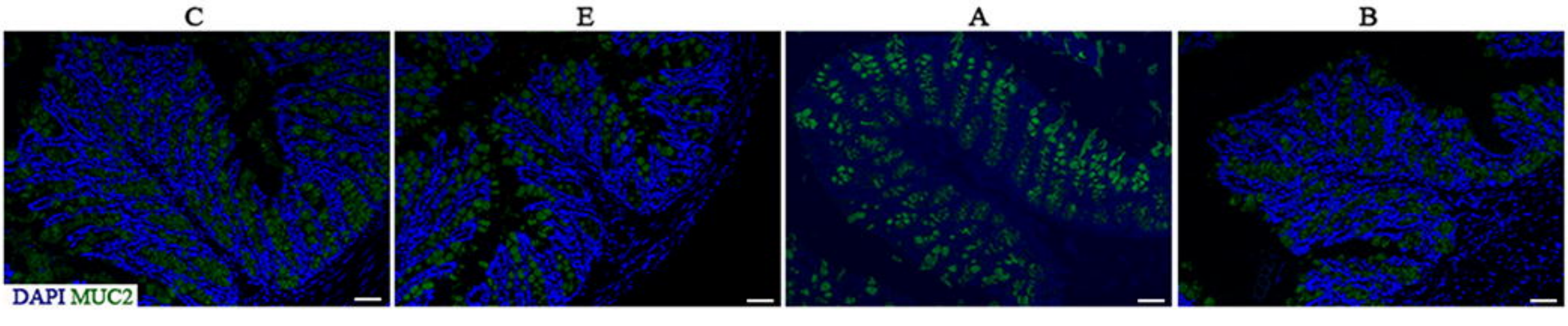

A

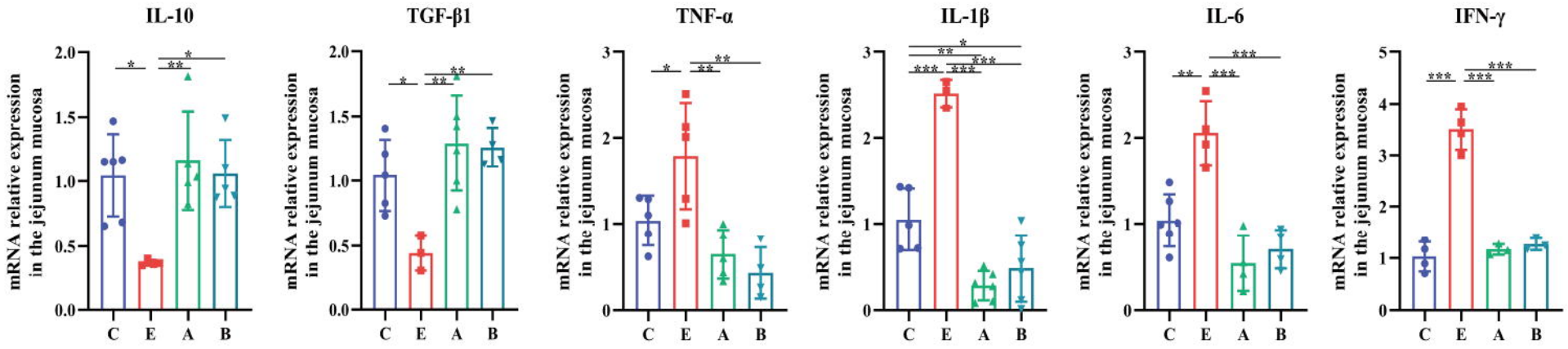

B

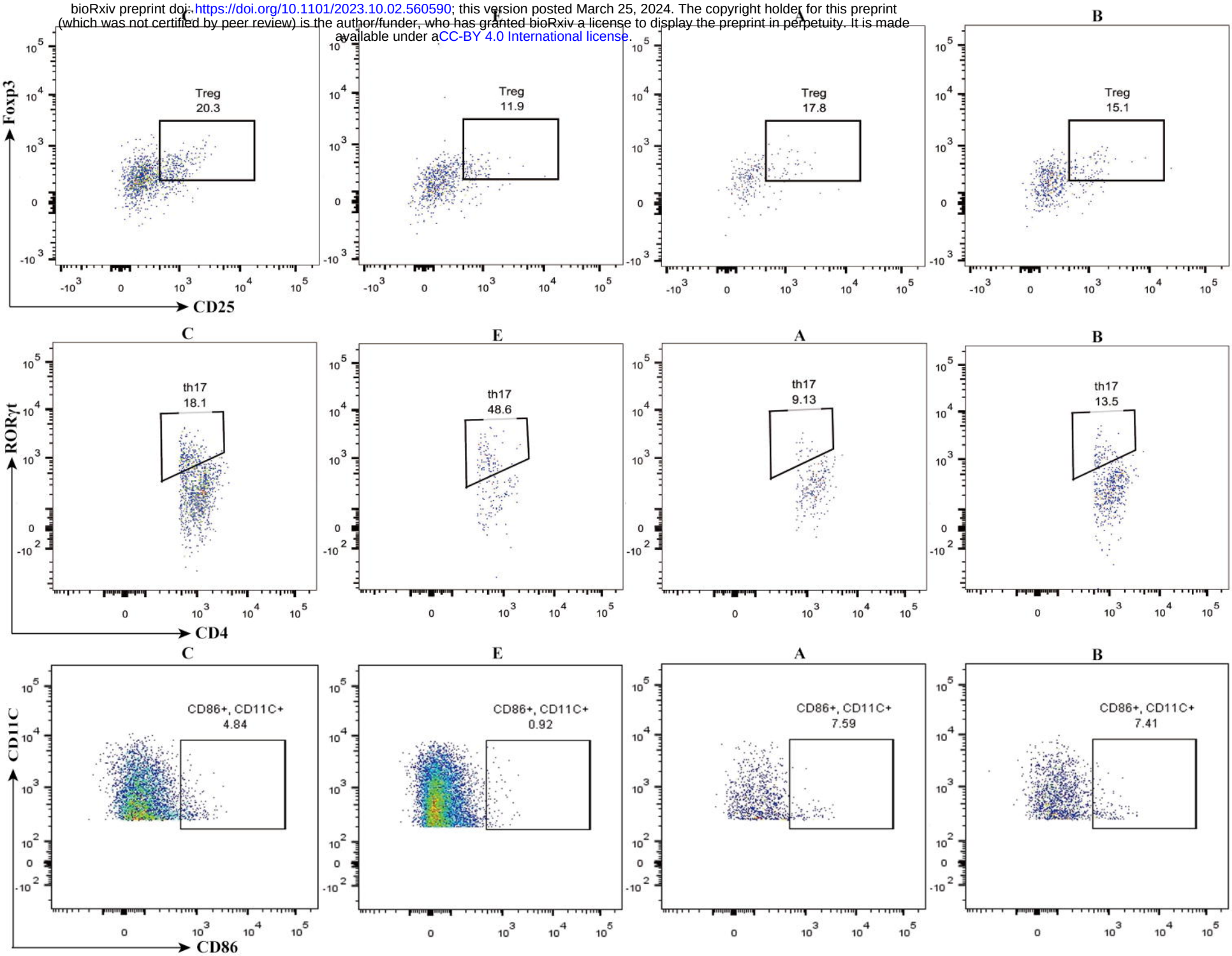

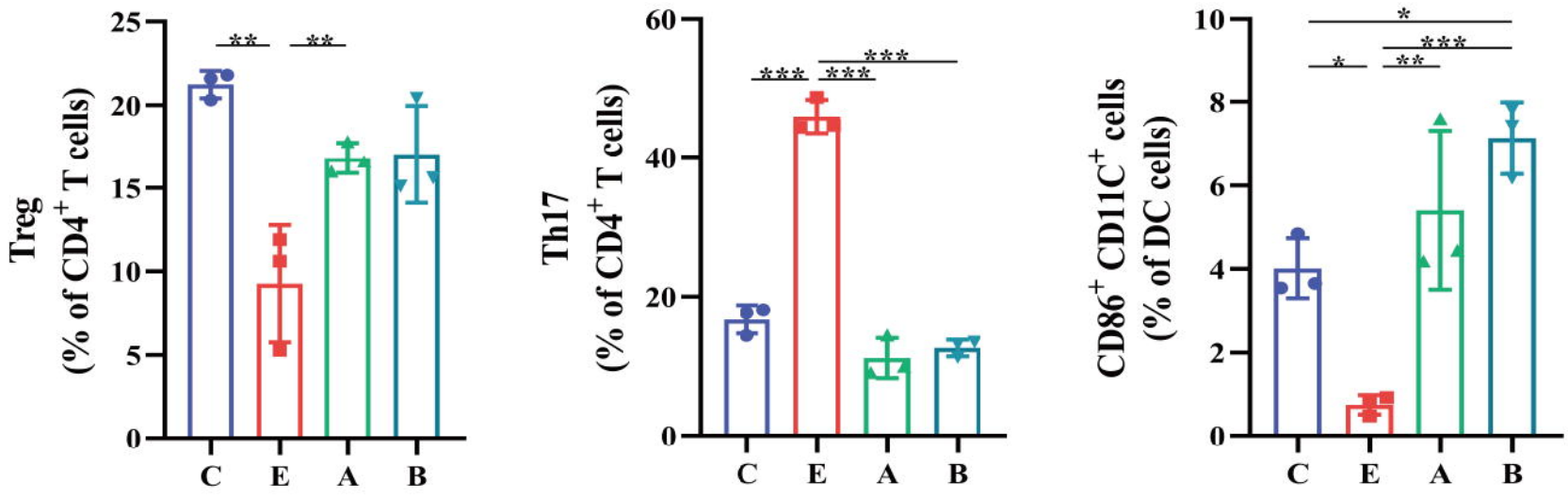

A

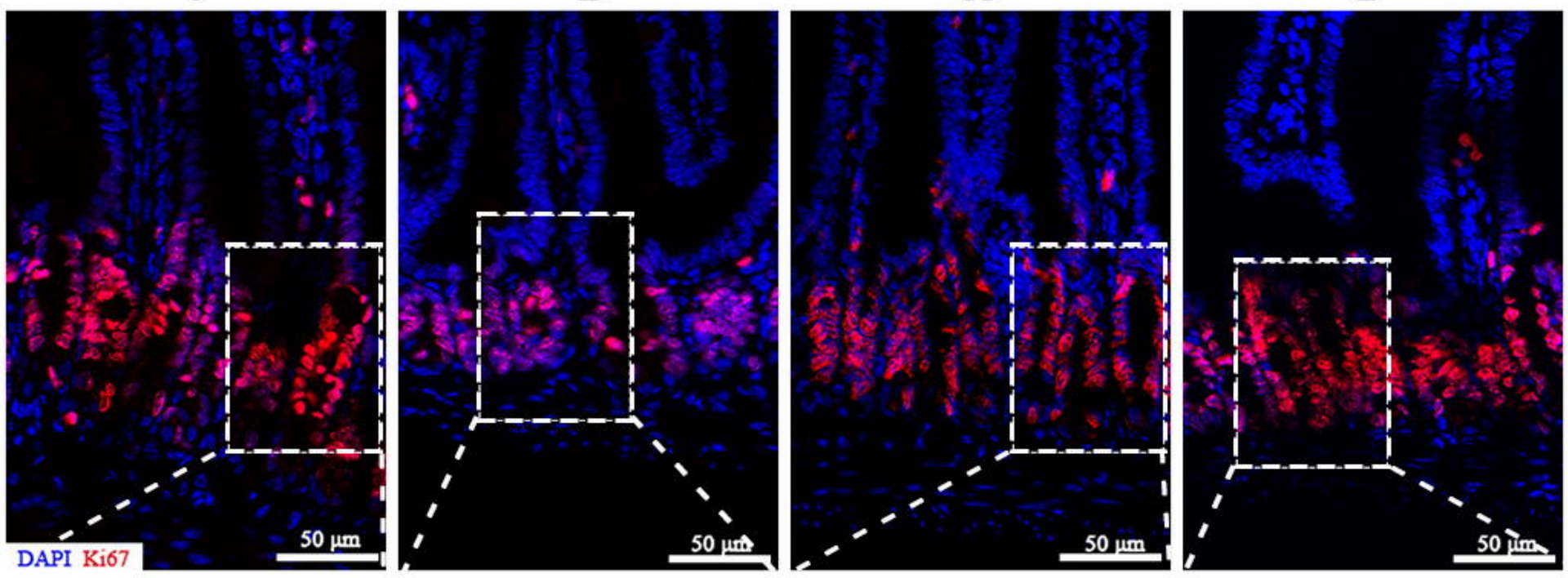

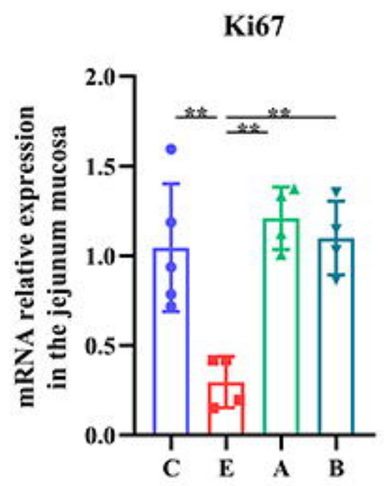

B

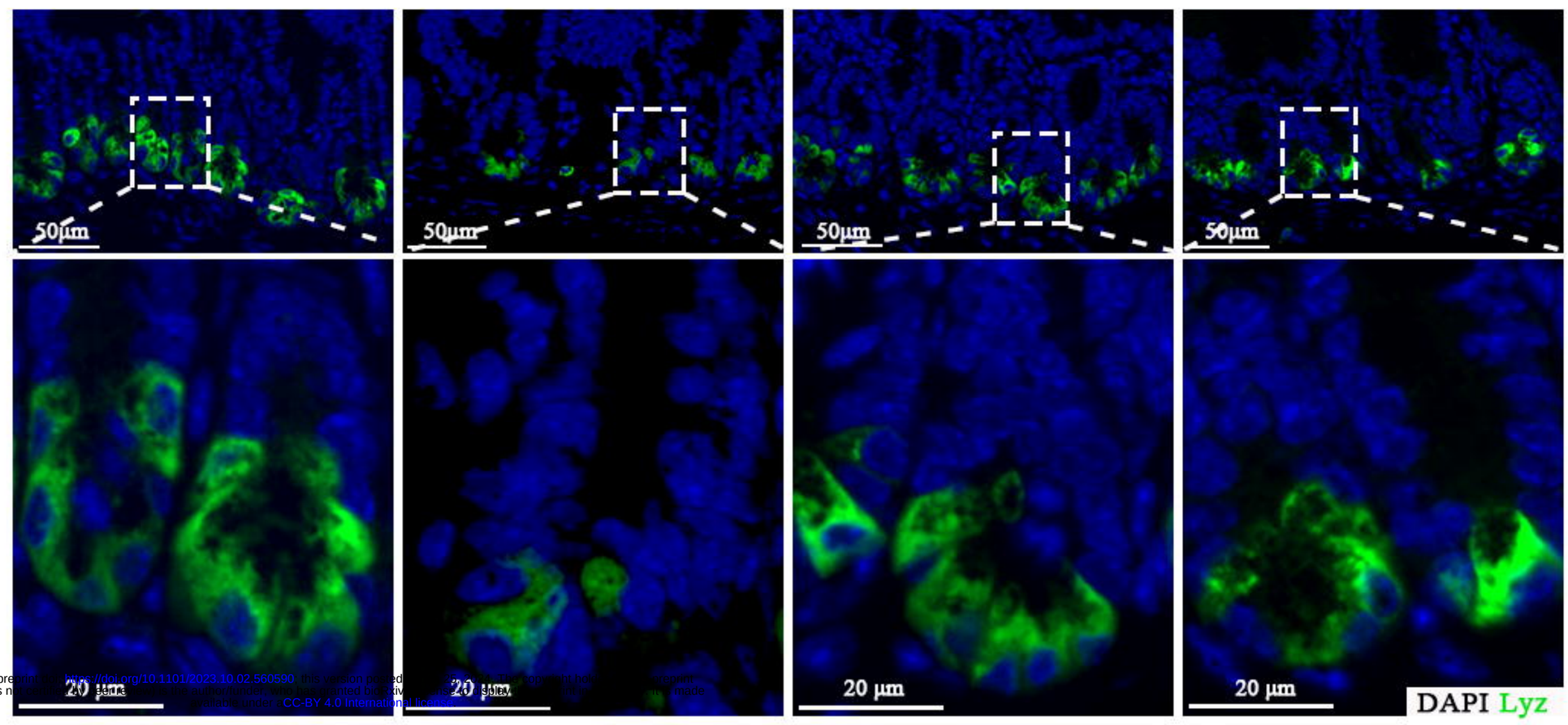

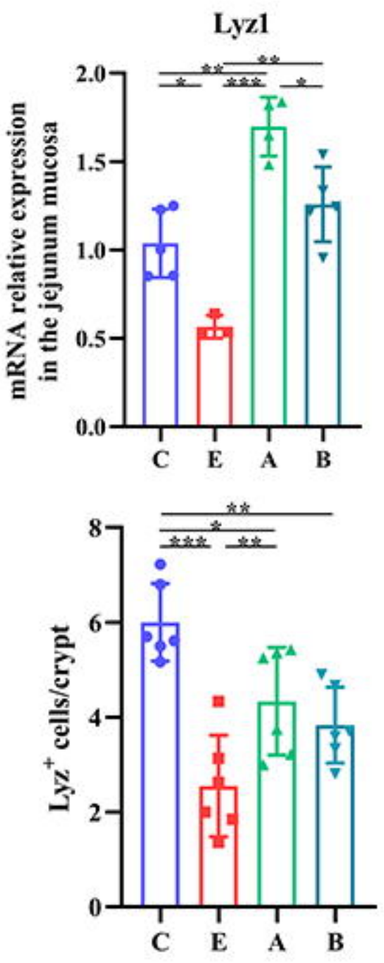

C

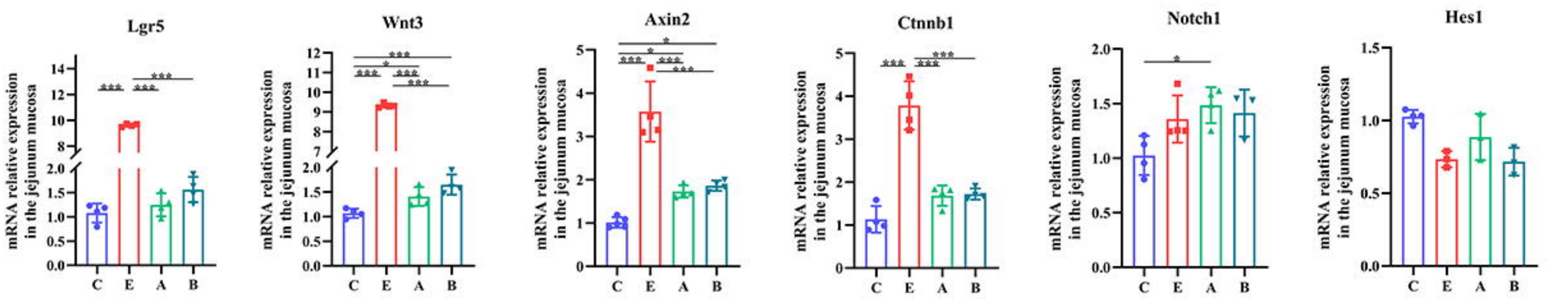

D

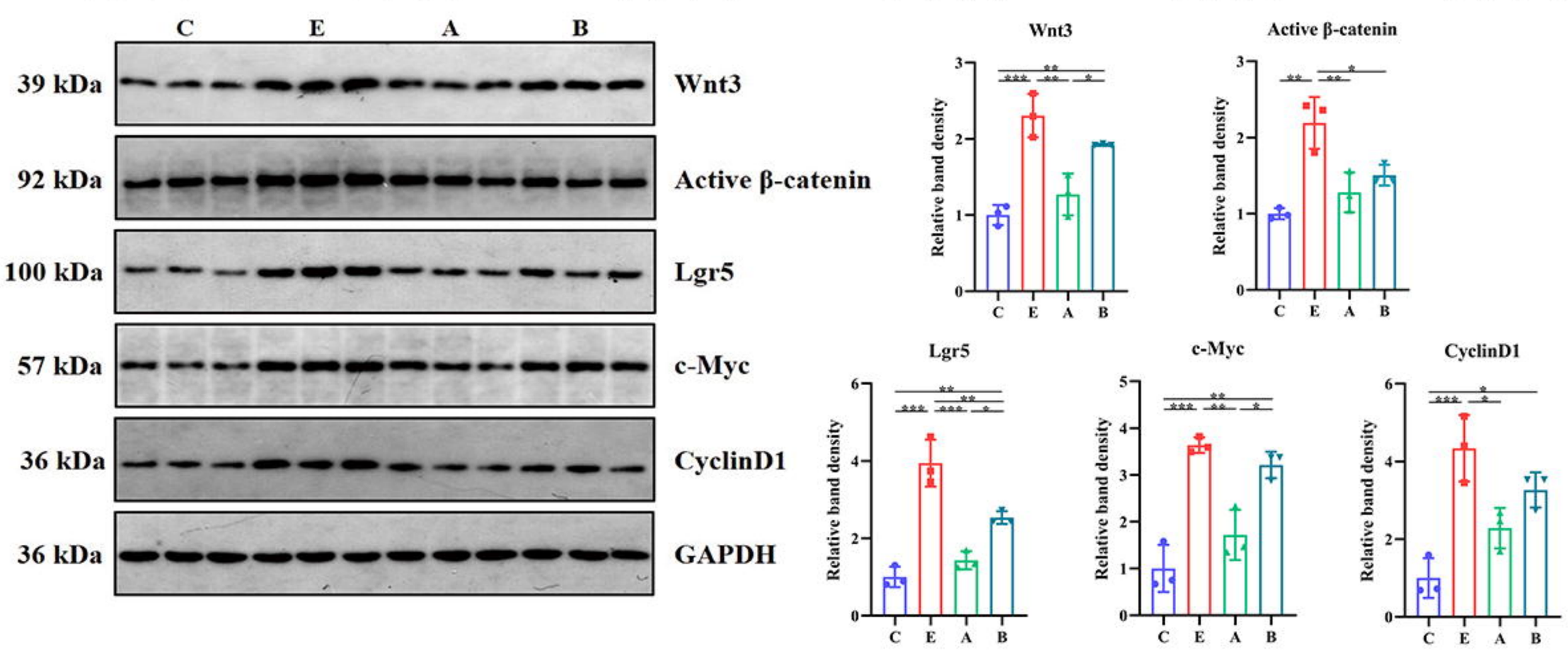

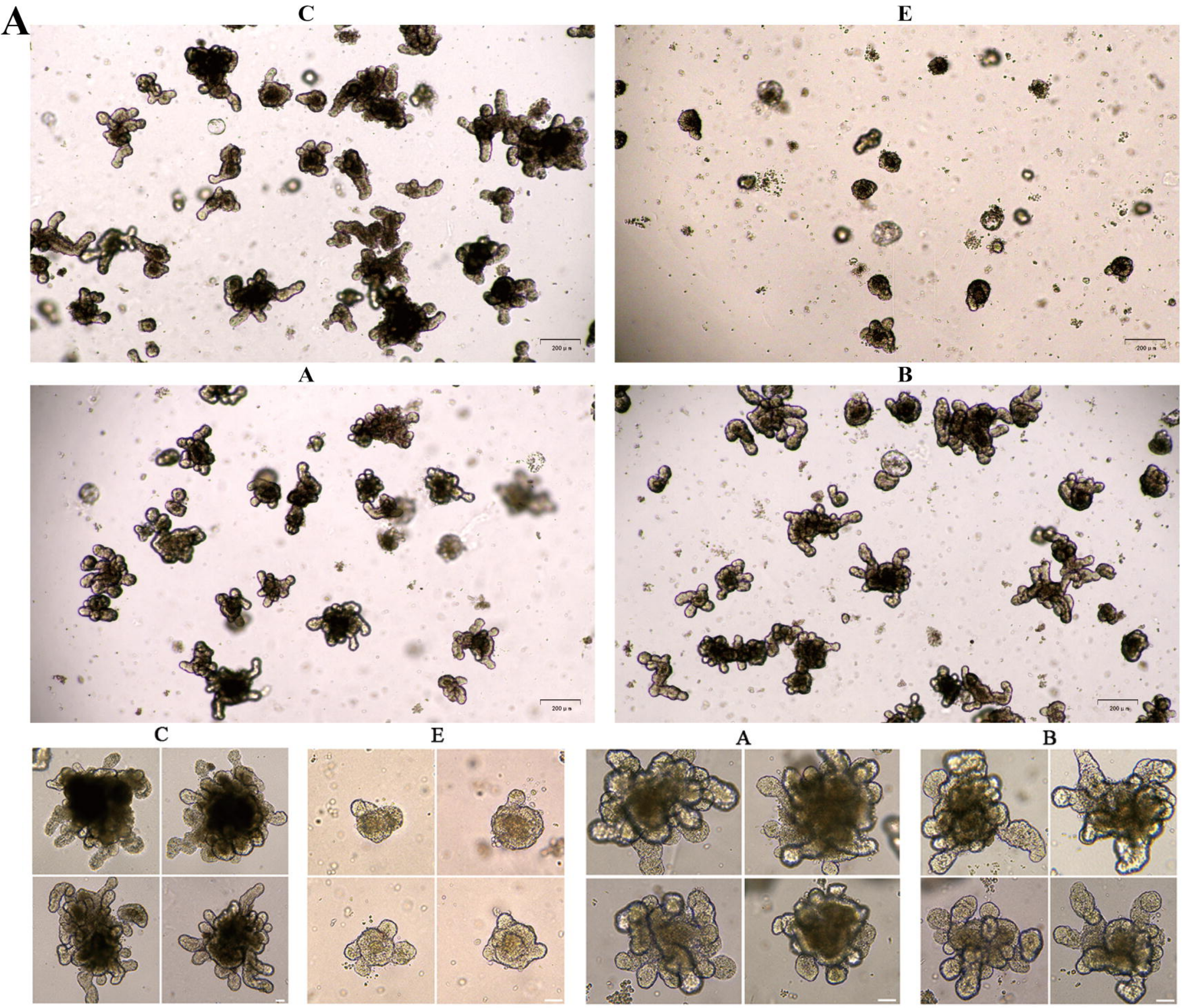

A

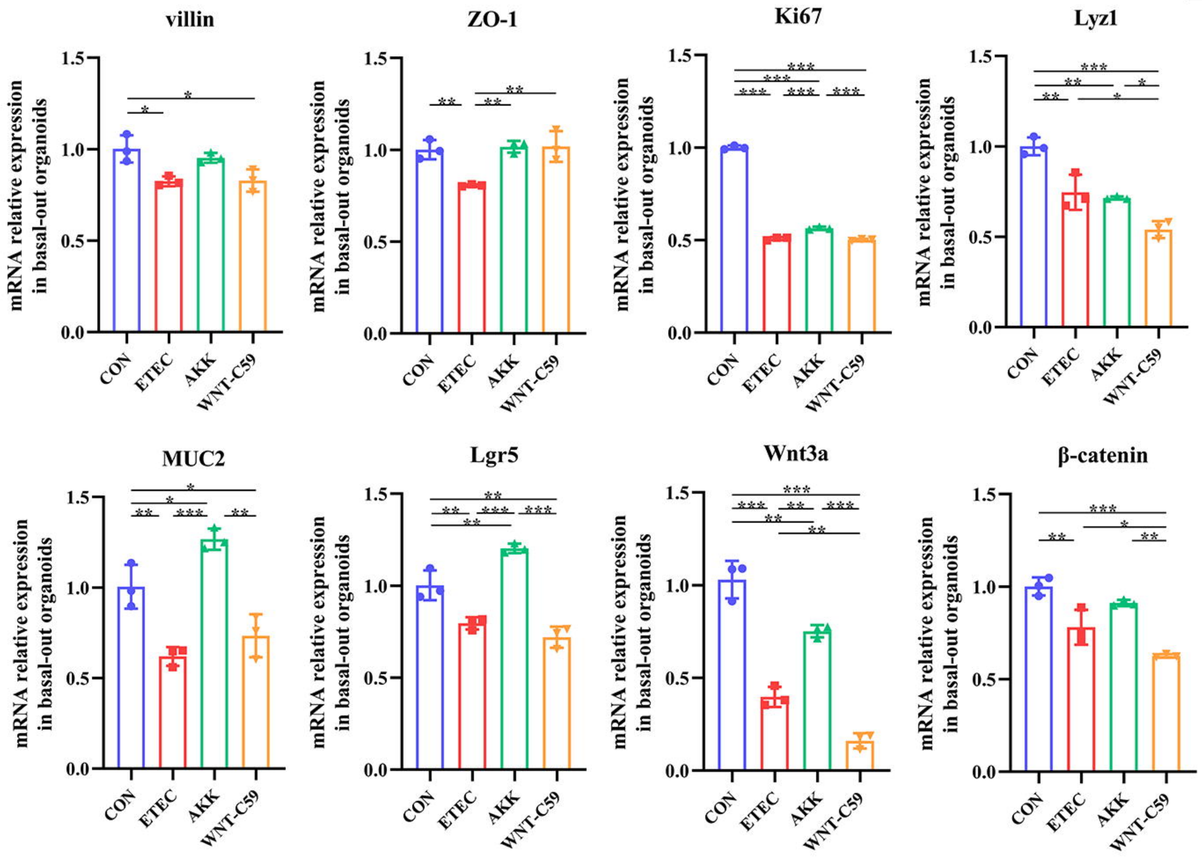

B

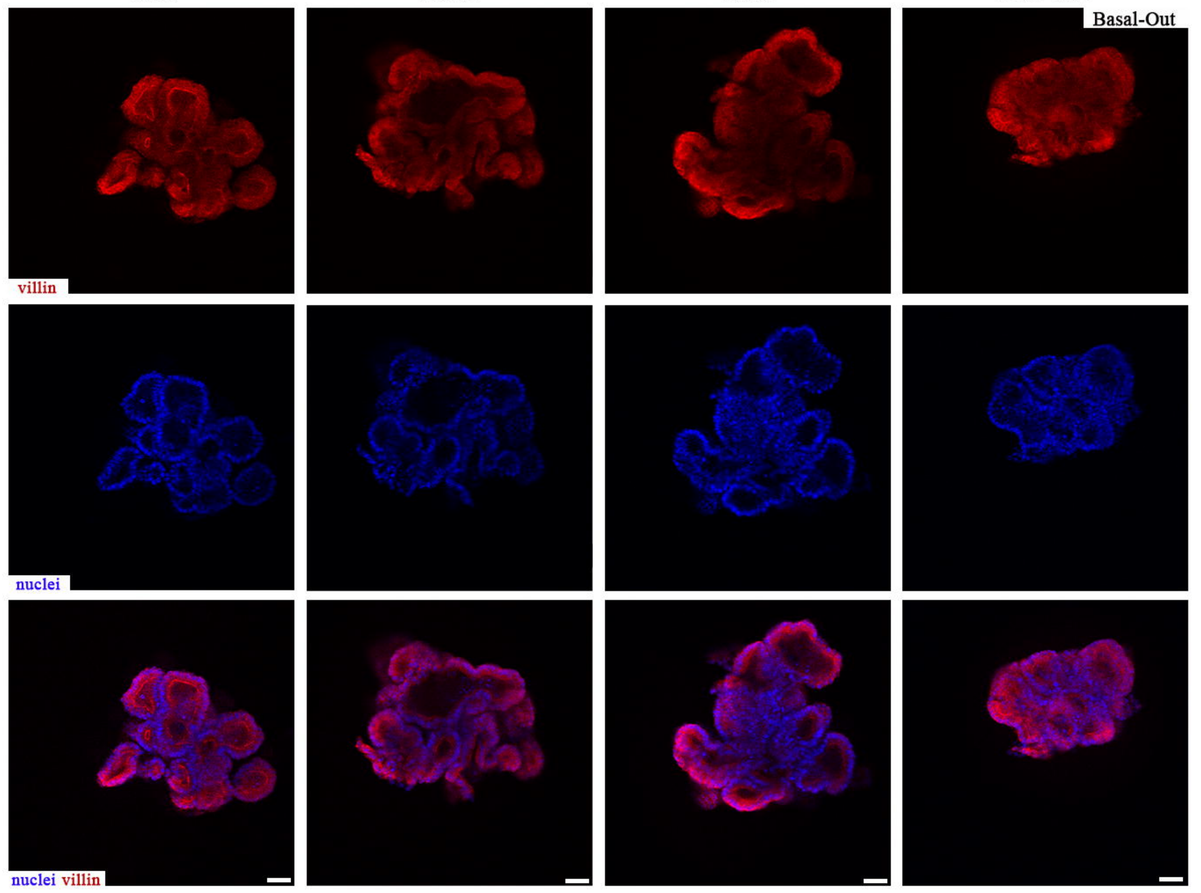

C

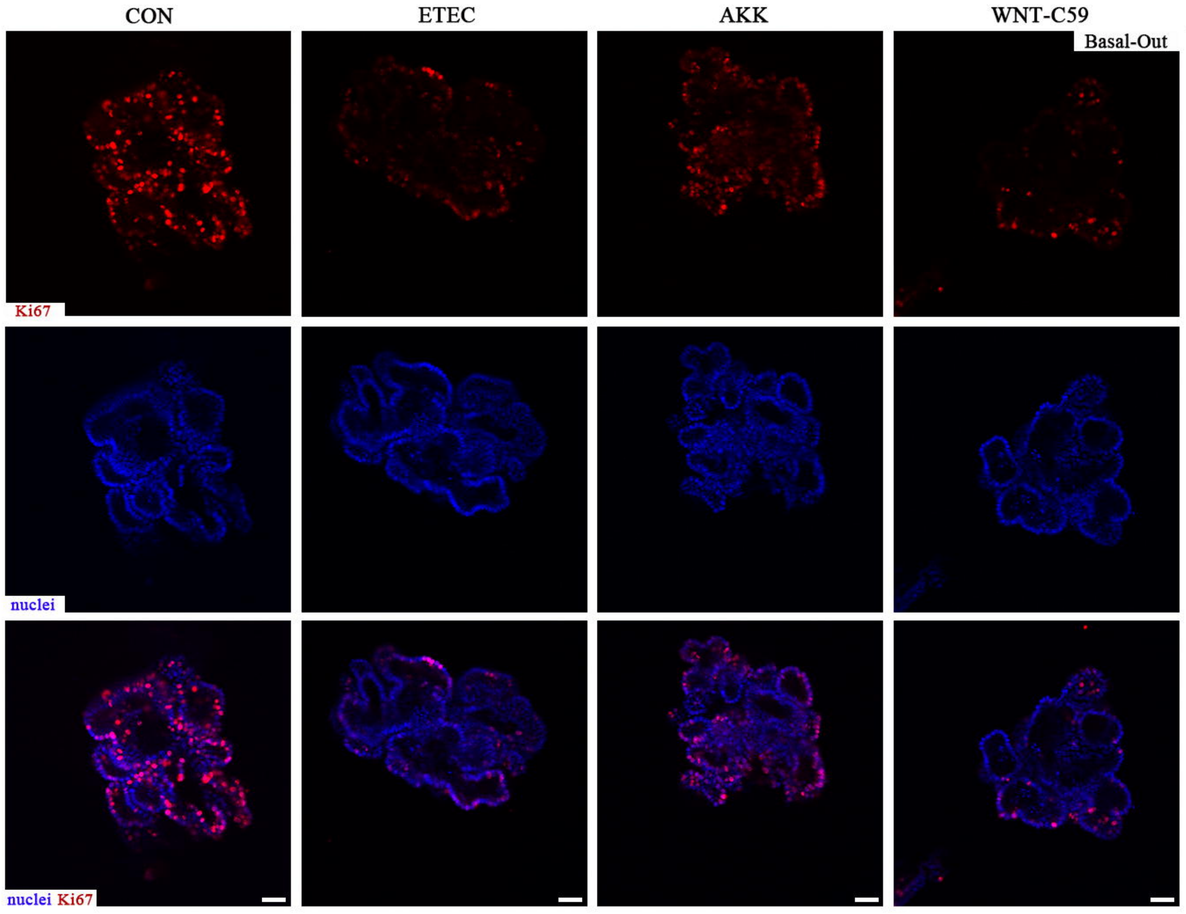

D

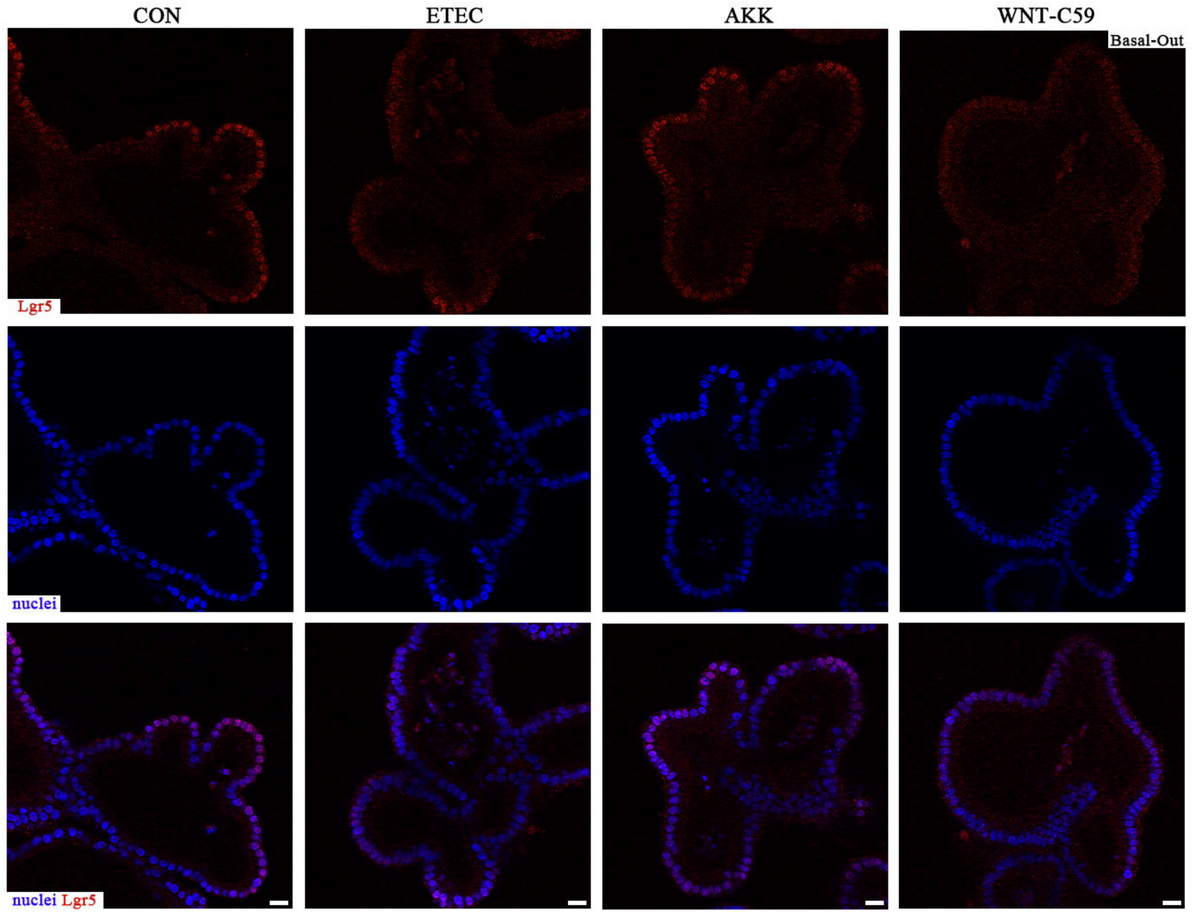

E

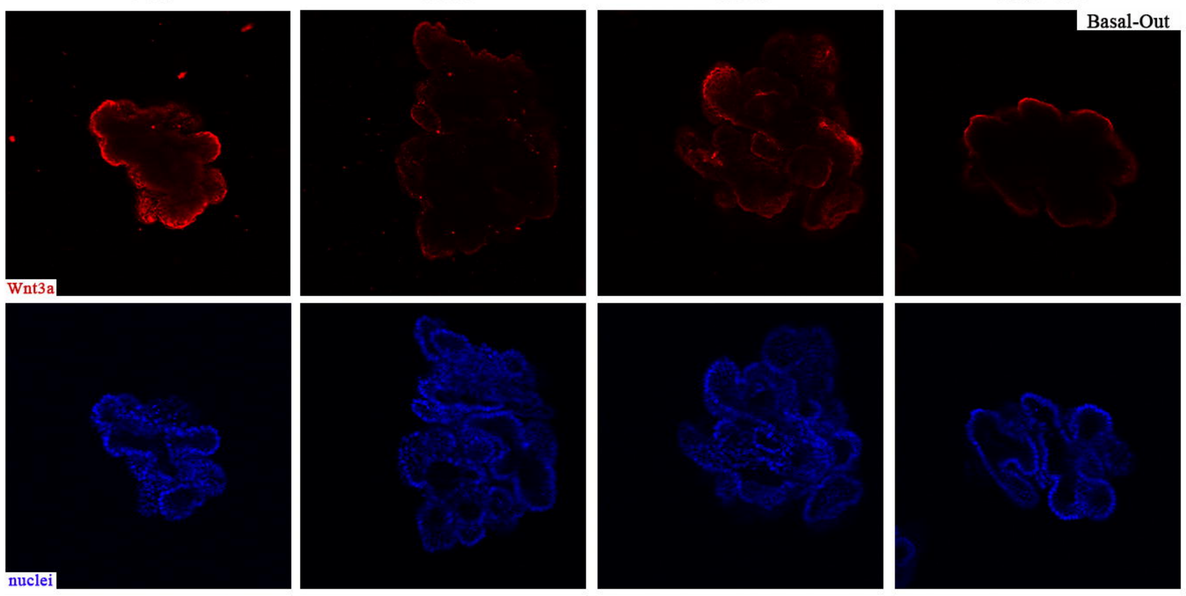

F

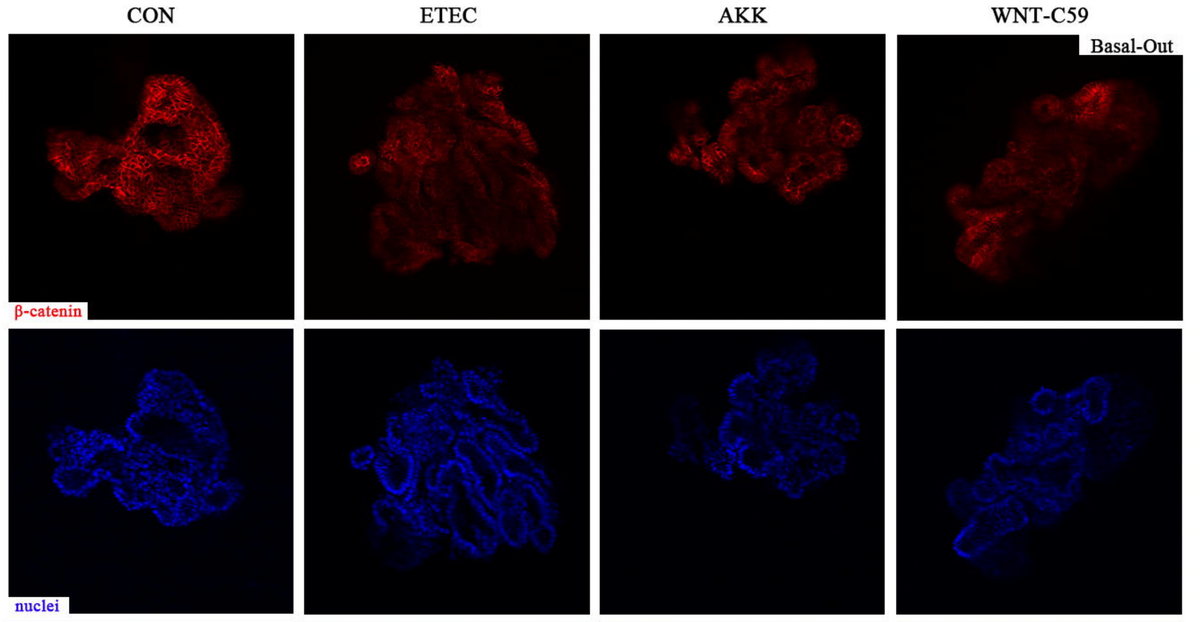

G

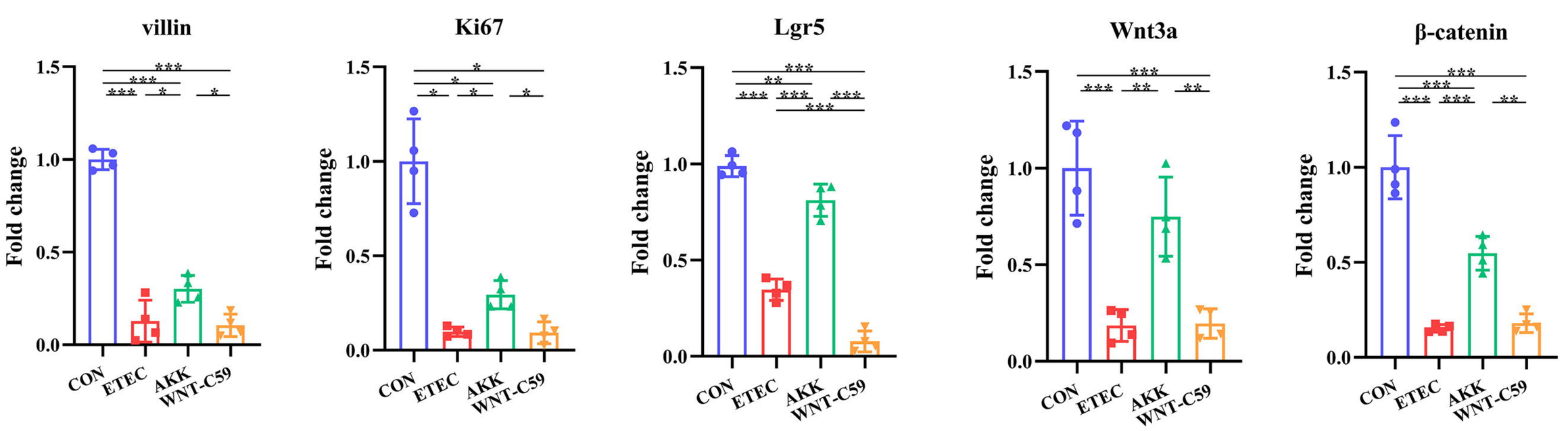

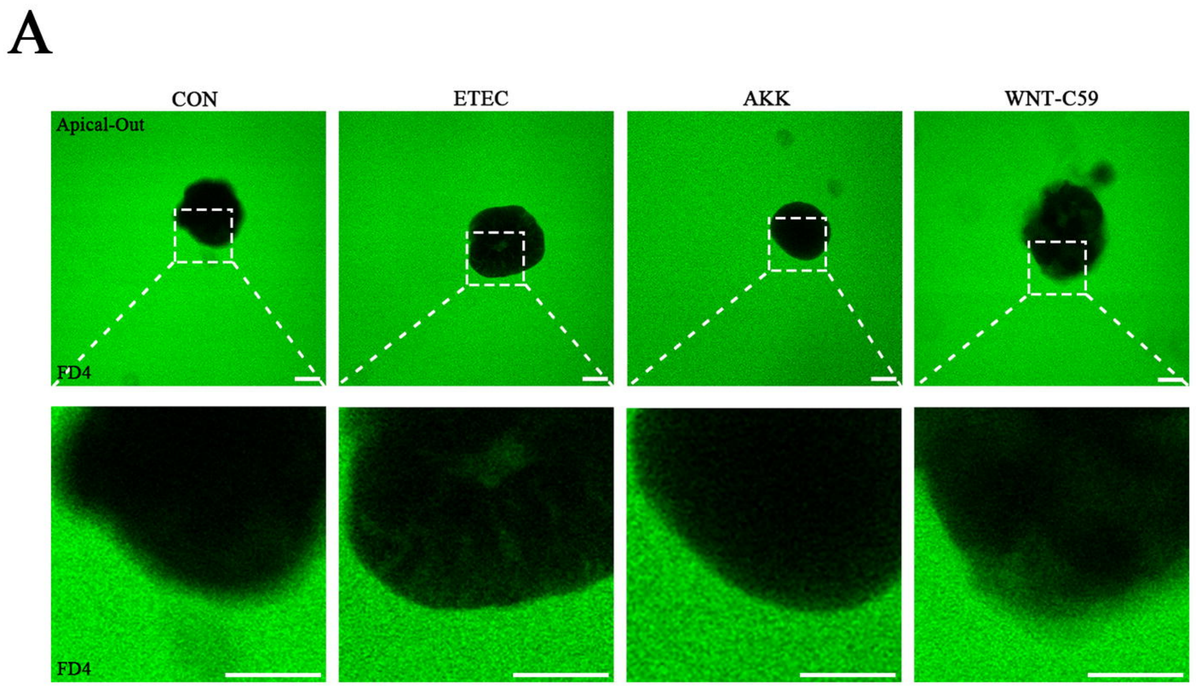
A
CON
ETEC
AKK
WNT-C59
Apical-Out
FD4
FD4

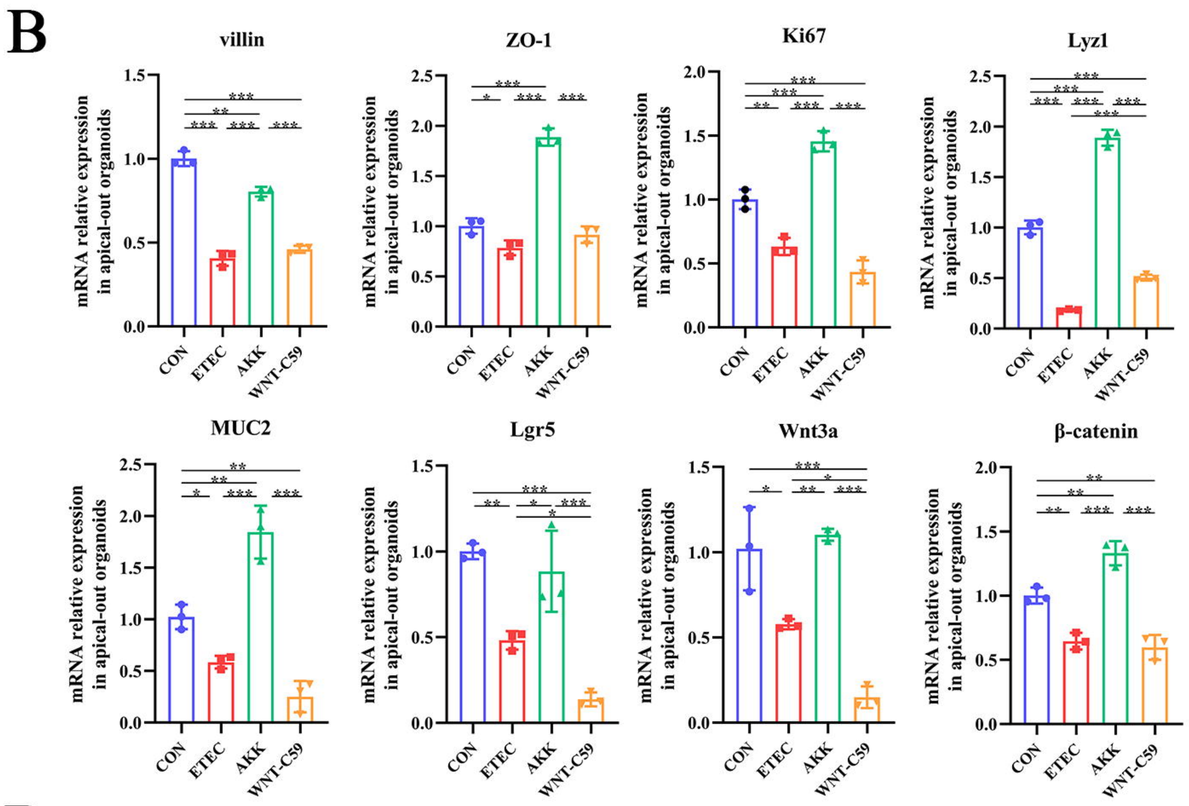
B
villin
ZO-1
Ki67
Lyz1
MUC2
Lgr5
Wnt3a
β-catenin
mRNA relative expression in apical-out organoids
CON
ETEC
AKK
WNT-C59

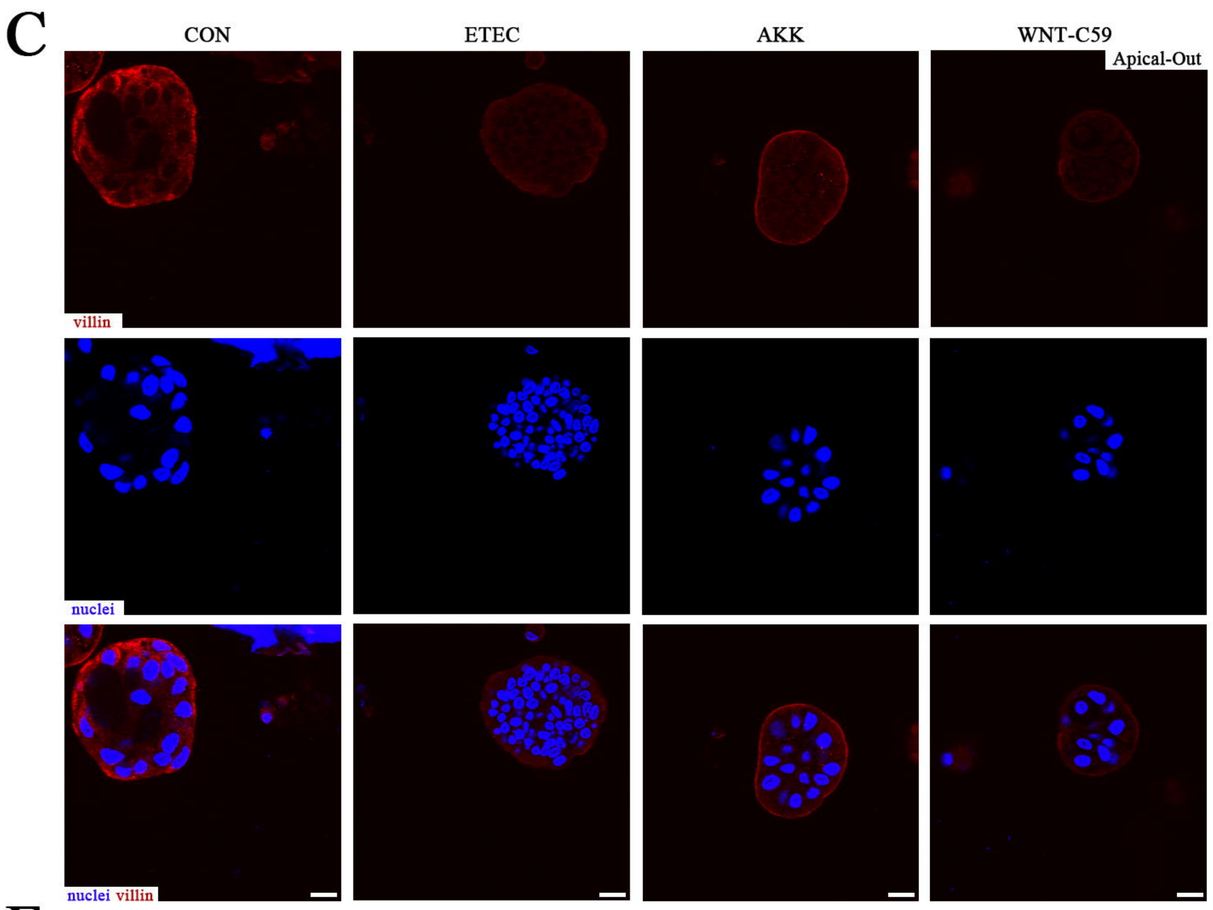
C
CON
ETEC
AKK
WNT-C59
Apical-Out
villin
nuclei
nuclei villin

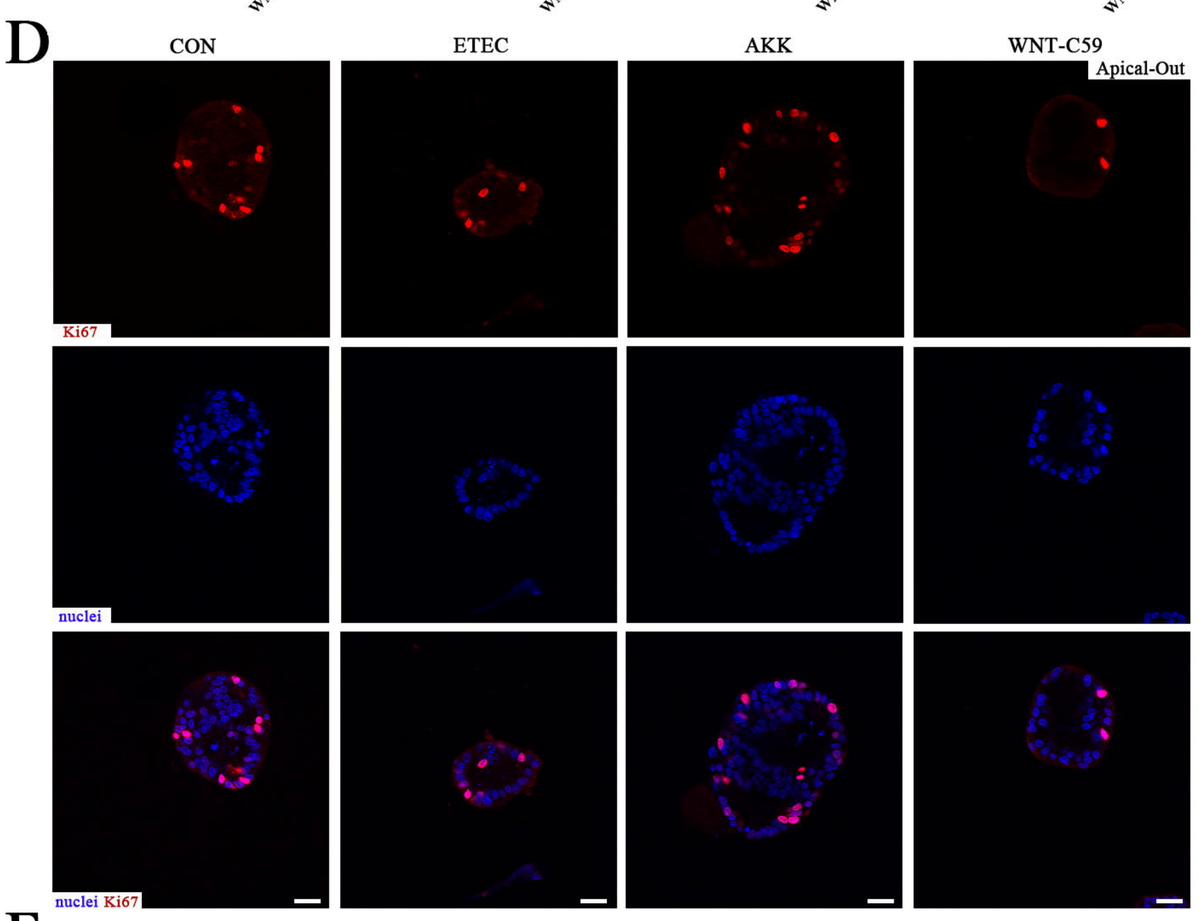
D
CON
ETEC
AKK
WNT-C59
Apical-Out
Ki67
nuclei
nuclei Ki67

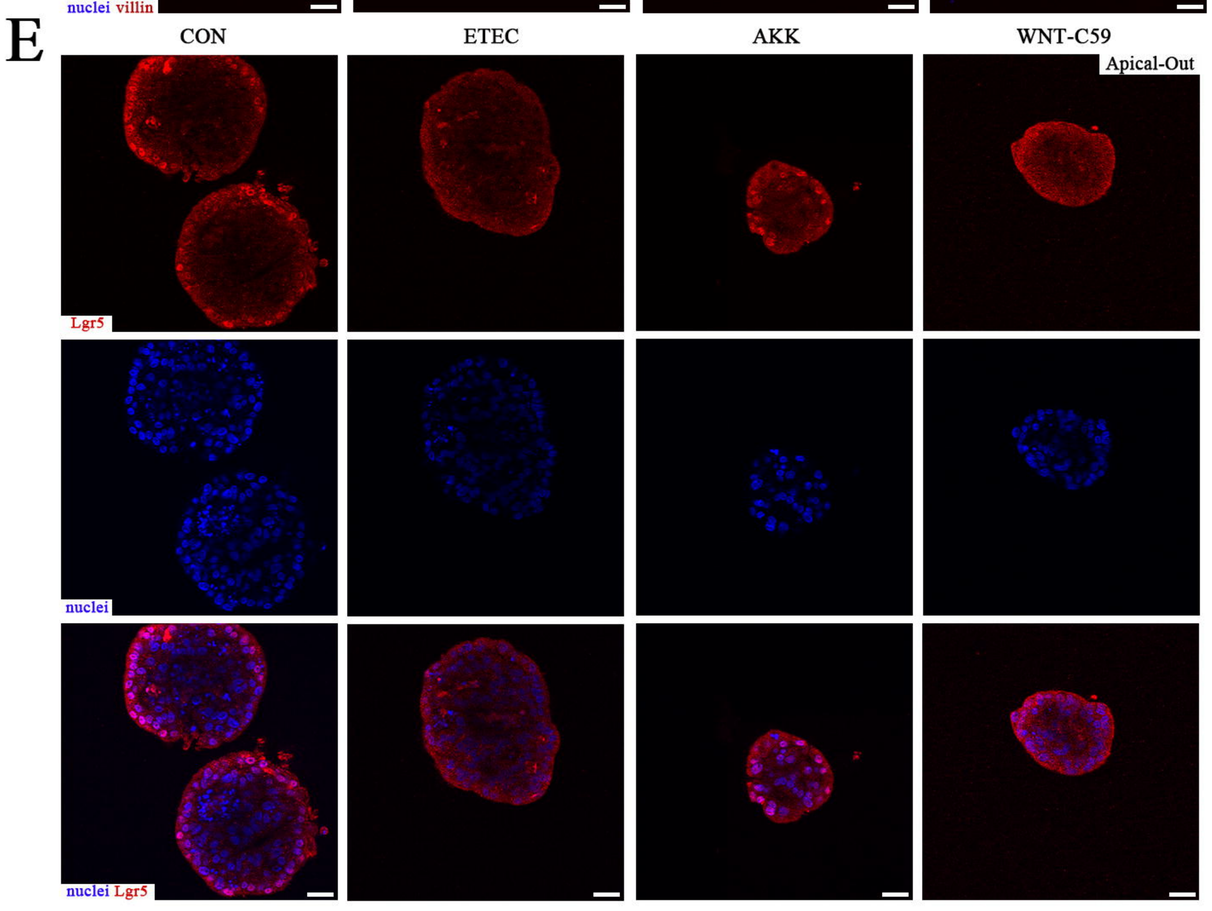
E
CON
ETEC
AKK
WNT-C59
Apical-Out
Lgr5
nuclei
nuclei Lgr5

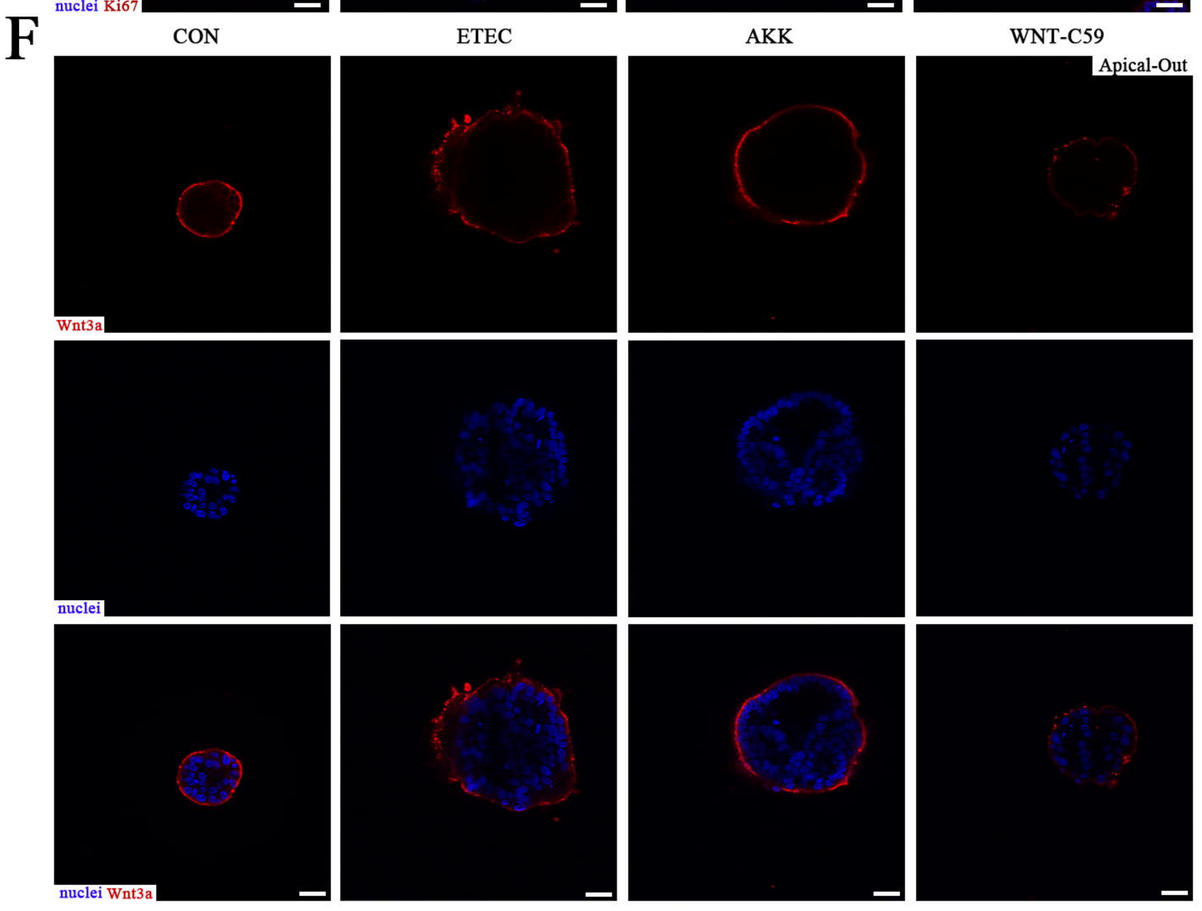
F
CON
ETEC
AKK
WNT-C59
Apical-Out
Wnt3a
nuclei
nuclei Wnt3a

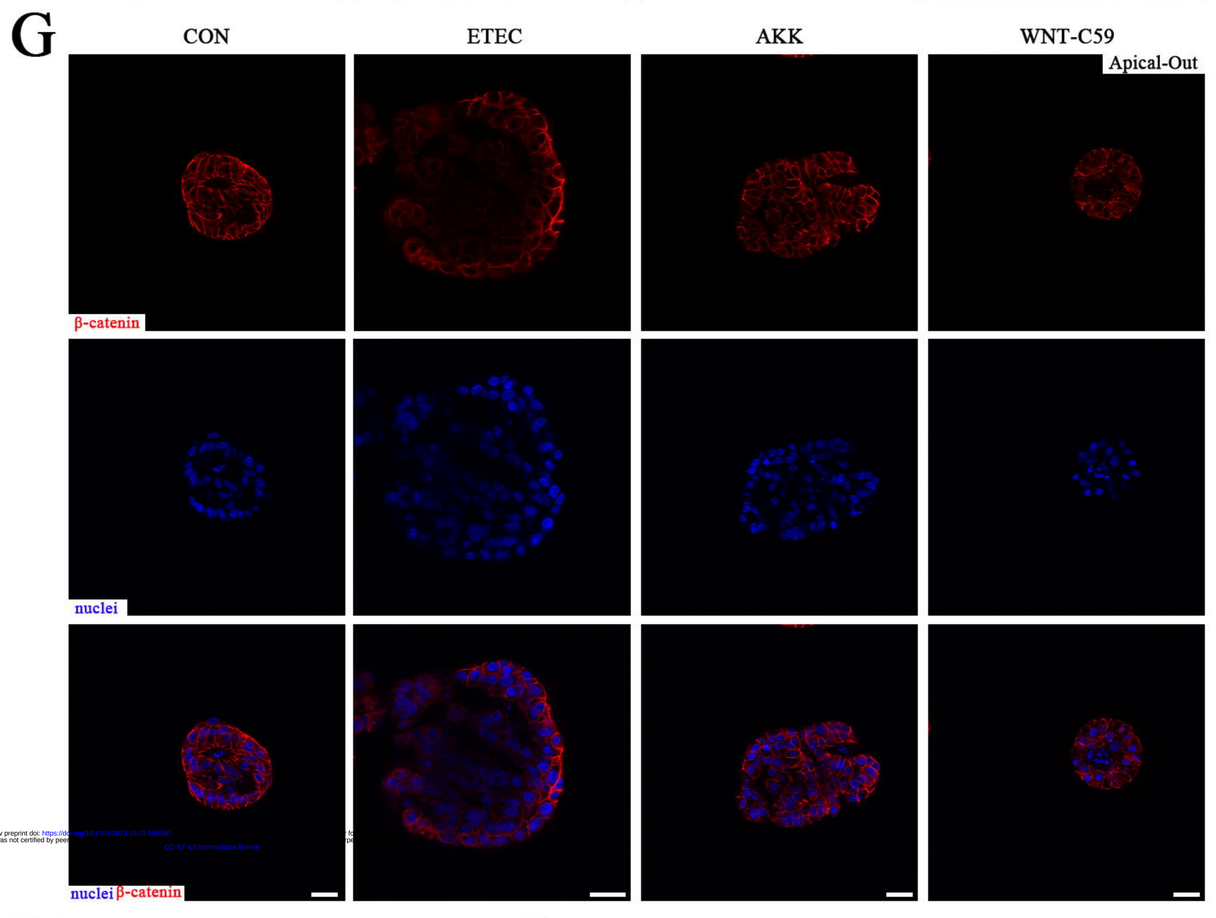
G
CON
ETEC
AKK
WNT-C59
Apical-Out
β-catenin
nuclei
nuclei β-catenin

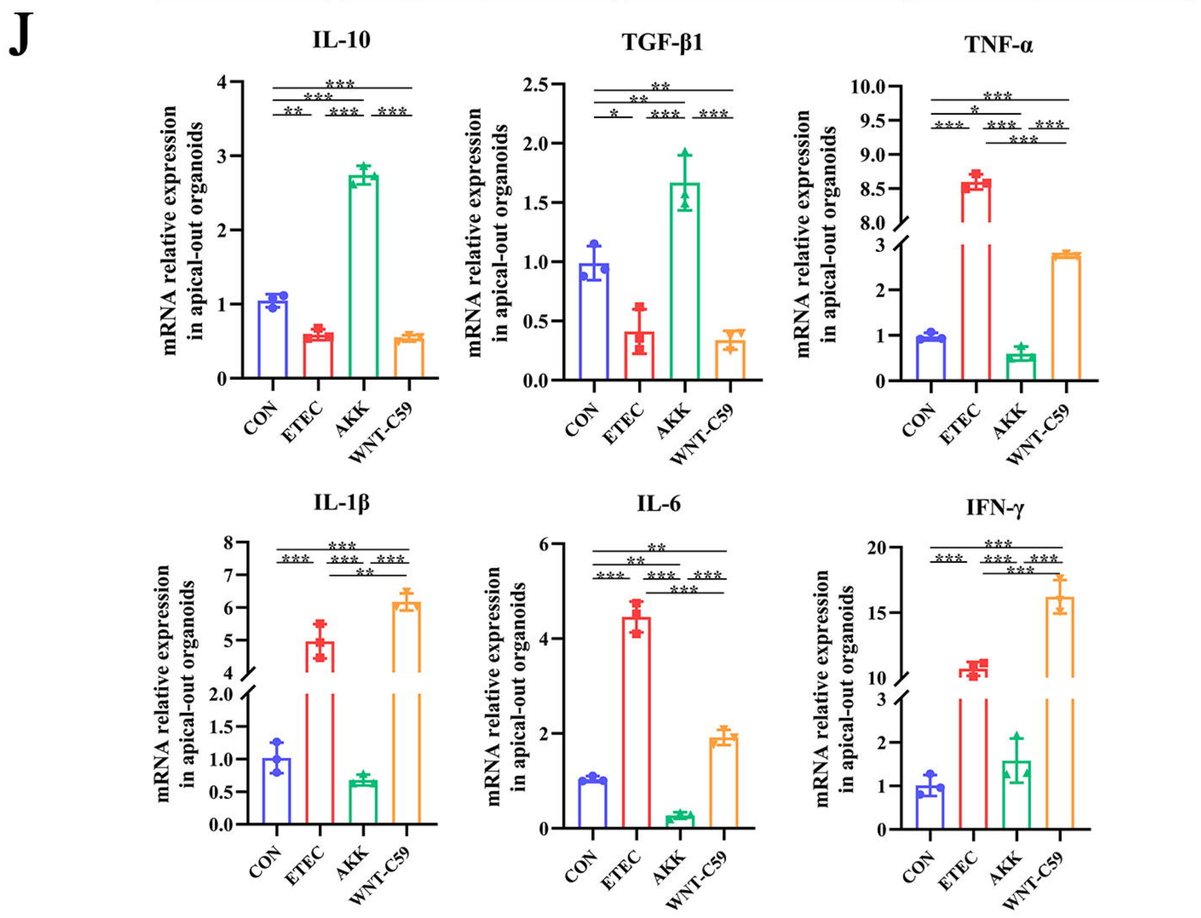
J
IL-10
TGF-β1
TNF-α
IL-1β
IL-6
IFN-γ
mRNA relative expression in apical-out organoids
CON
ETEC
AKK
WNT-C59

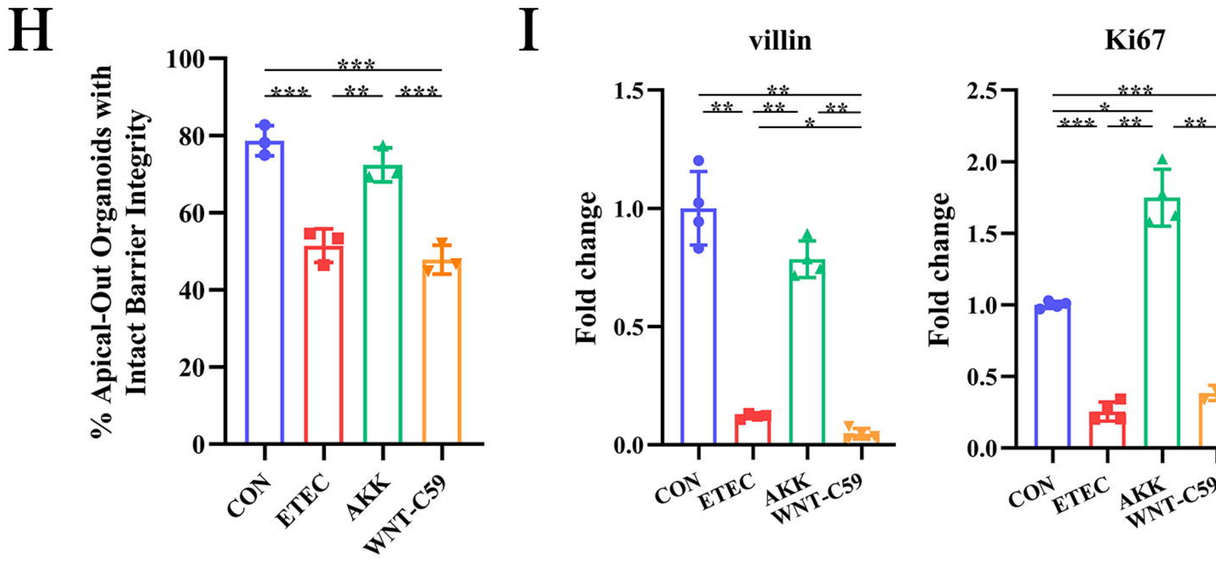
H
% Apical-Out Organoids with Intact Barrier Integrity
CON
ETEC
AKK
WNT-C59

I
villin
Ki67
Lgr5
Wnt3a
β-catenin
Fold change
CON
ETEC
AKK
WNT-C59